Electronic Supplementary Material (ESI) for Polymer Chemistry.

Electronic Supporting Information

Ugi multicomponent reaction to prepare peptide-peptoid hybrid structures with diverse chemical functionalities

Manuel Hartweg[1], Charlotte J. C. Edwards-Gayle[2,3], Elham Radvar[1], Dominic Collis[1], Mehedi Reza[4], Michael Kaupp[5,6], Jan Steinkönig[5,6], Janne Ruokolainen[4], Robert Rambo,[3] Christopher Barner-Kowollik[5,6], Ian W. Hamley[2], Helena S. Azevedo[1], and C. Remzi Becer[1]*

[1] Polymer Chemistry Laboratory, School of Engineering and Materials Science, Queen Mary University of London, London, E1 4NS, UK

[2] Department of Chemistry, University of Reading, Whiteknights, Reading, RG6 6AD, UK

[3] Diamond Light Source Ltd, Harwell Science & Innovation Campus, Didcot OX11 0DE, UK

[4] Department of Applied Physics, Aalto University, Finland

[5] Preparative Macromolecular Chemistry, Institut für Technische Chemie und Polymerchemie, Karlsruhe Institute of Technology (KIT), Engesserstraße 18, 76128 Karlsruhe, Germany and Institute of Biological Interfaces, Karlsruhe Institute of Technology (KIT), Hermann-von-Helmholtz-Platz 1, 76344 Eggenstein-Leopoldshaven, Germany

[6] School of Chemistry, Physics and Mechanical Engineering, Queensland University of Technology (QUT), 2 George Street, QLD 4000, Brisbane, Australia

Corresponding author: r.becer@qmul.ac.uk

Supplementary Information Contents

1 Nomenclature of *Ugi* peptoids and peptide-*Ugi* peptoid hybrids 4

2 Experimental Section 5

2.1 Materials, General Methods and Instrumentation 5

2.2 Synthesis of Monomers 8

2.2.1 Synthesis of Polystyrene Butyl Amine Resin 8

2.2.2 Synthesis of (2*R*,4*S*,5*R*)-2-(acetoxymethyl)-6-((3-oxopropyl)thio)tetra-hydro-2*H*-pyran-3,4,5-triyl triacetate 8

2.2.3 Synthesis of MeO-PEG$_{550}$-CHO 11

3 Synthesis and Characterisation of Oligomers 14

3.1 General Procedures 14

3.2 Characterisation of Oligomers 16

3.2.1 Characterisation of H_2N-F(*n*Pr,Cy)-F-G-F-$CONH_2$ 1: 16

3.2.2 Characterisation of H_2N-F($C_{10}H_{21}$,Cy)-F-G-F-$CONH_2$ 2: 18

3.2.3 Characterisation of H_2N-F-F(*n*Pr,Cy)-K-K-K-K-$CONH_2$ 3: 20

3.2.4 Characterisation of H_2N-F-F(*n*Pr,Cy)-K-K-K-K-$CONH_2$ 4: 22

3.2.5 Characterisation of H_2N-F(CH_2)$_2$-S-Glu(OAc_4),Cy)-K-K-K-K-$CONH_2$ 5: 24

3.2.6 Characterisation of Fmoc-F(PEG_{550},Cy)-K-K-K-K-$CONH_2$ 6: 25

3.2.7 Characterisation of H_2N-F($C_{10}H_{21}$,Cy)-F-F(*n*Pr,Cy)-F-F($C_{10}H_{21}$,Cy)-F-G-F-$CONH_2$ 7: 27

3.2.8 Characterisation of Fmoc-F(*n*Pr,Cy)-F-F(*n*Pr,Cy)-F-F(*n*Pr,Cy)-K-K-K-K-$CONH_2$ 8: 29

3.2.9 Characterisation of H_2N-K(CH_2)$_2$-S-Glu),Cy)-K(CH_2)$_2$-S-Glu),Cy)-K(CH_2)$_2$-S-Glu),Cy)-K-K-K-K-$CONH_2$ 9: 31

3.2.10 Characterisation of H_2N-F($C_{10}H_{21}$,Cy)-G($C_{10}H_{21}$,Cy)-F($C_{10}H_{21}$,Cy)NH 10: 33

3.2.11 Characterisation of Fmoc-G($C_{10}H_{19}$,Cy)-G(*n*Pr,Cy)-F($C_{10}H_{21}$,Cy)-G($C_{10}H_{21}$,Cy)-F(*n*Pr,4-EM)- F($C_{10}H_{19}$,Cy)NH 11: 35

3.2.12 Characterisation of H_2N-F($C_{10}H_{19}$,Cy)-(F($C_{10}H_{19}$,Cy))$_5$-F($C_{10}H_{19}$,Cy)NH 12: 36

4 Tandem MS analysis 37

4.1 Analysis of H_2N-F(*n*Pr,Cy)-F-G-F-$CONH_2$ 1: 37

4.2 Analysis of H_2N-F($C_{10}H_{21}$,Cy)-F-G-F-$CONH_2$ 2: 38

4.3 Analysis of H_2N-F-F(*n*Pr,Cy)-K-K-K-K-$CONH_2$ 3: 39

4.4 Analysis of H_2N-F($C_{10}H_{21}$,Cy)-F-F(*n*Pr,Cy)-F-F($C_{10}H_{21}$,Cy)-F-G-F-$CONH_2$ 7: 40

4.5 Analysis of Fmoc-F(*n*Pr,Cy)-F-F(*n*Pr,Cy)-F-F(*n*Pr,Cy)-K-K-K-K-$CONH_2$ 8: 41

4.6 Analysis of H_2N-K(CH_2)$_2$-S-Glu),Cy)-K(CH_2)$_2$-S-Glu),Cy)-K(CH_2)$_2$-S-Glu),Cy)-K-K-K-K-$CONH_2$ 9: 43

4.7 Analysis of H_2N-F($C_{10}H_{21}$,Cy)-G($C_{10}H_{21}$,Cy)-F($C_{10}H_{21}$,Cy)NH 10: 44
5 Assembly studies 45

1 Nomenclature of *Ugi* peptoids and peptide-*Ugi* peptoid hybrids

The nomenclature of *Ugi* units is less trivial than the one for conventional peptides (**Figure S1**, **a**) or polyglycinic peptoids (**Figure S1**, **b**) or respective hybrid structures (**Figure S1**, **c**). This is because any possible amino acid may be employed in the reaction – not only glycine and its derivatives. Furthermore, the *Ugi*-MCR provides two additional R-groups based on the aldehyde and isonitrile. In an *Ugi* peptoid unit the employed amino acid (**Figure S1**, **c**, blue) builds the peptoid backbone. The pendant group at the amide nitrogen is composed of the main part of the actual *Ugi* scaffold (red), which still carries the R-groups of the aldehyde (light blue) and isocyanide (marine blue). As the orange scaffold is repetitive throughout every *Ugi* sequence, it does not occur separately in the nomenclature of *Ugi* peptoid units. However, the structure of the aldehyde and isocyanide are reported in the nomenclature of those structures. A representative example is discussed (**Figure S1**, **e**). Conventional peptide sequences (green) maintain their single letter code without any change. When an *Ugi* peptoid sequence is described, amino acids (blue) keeps their letter code (in comparison to the nomenclature of polyglycines), as all available amino acids can be incorporated and not only glycines. Then, in brackets the R-group of the aldehyde (light blue) is reported first (caution: when *e.g.* butyraldehyde H_3C-$(CH_2)_2$-CHO is employed, it loses the aldehyde carbon in the nomenclature and is reported as *n*Pr consequently). Second, the R-group of the isocyanide is reported in the bracket. Thereby, the R-group is described as attached to the isocyanide.

Example:

Starting compound	PG-Lys-OH	Undecanal H_3C-$(CH_2)_9$-CHO	Cyclohexyl isocyanide CyNC
Code in a sequence	PG-K-OH	$C_{10}H_{21}$	Cy
Description of the sequence	PG-K($C_{10}H_{21}$, Cy)-OH		

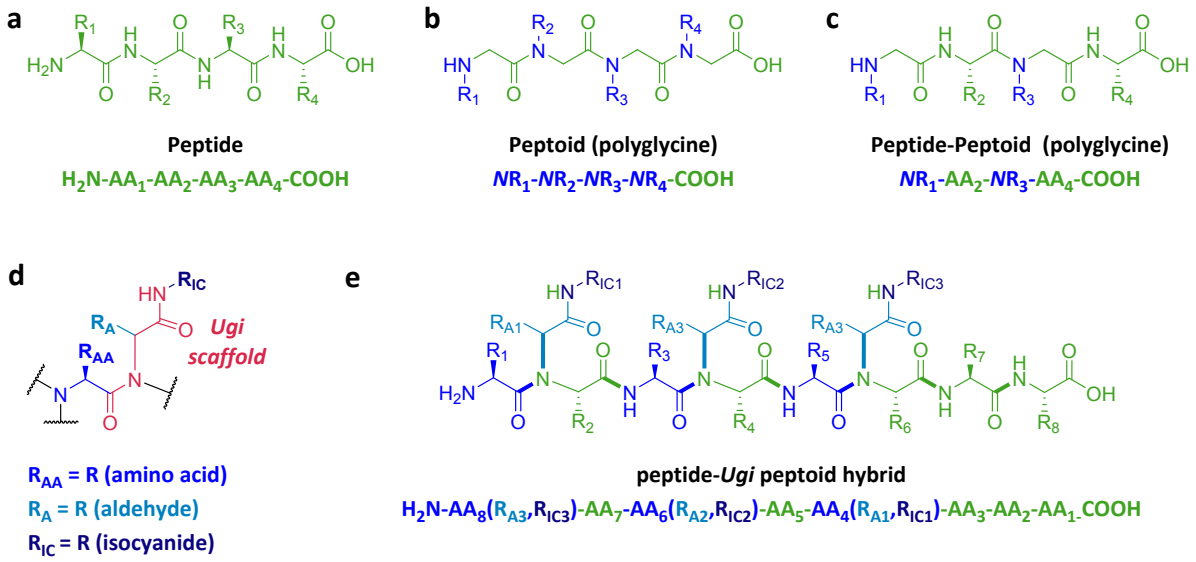

Figure S1 | Nomenclature of Ugi-peptoids and peptide-peptoid hybrids. a. Structure of a conventional peptide and its nomenclature as single letter code. **b.** Structure of a conventional peptoid (polyglycine) and its nomenclature as letter code. **c.** Structure of a peptide-peptoid (polyglycine) hybrid and its nomenclature as letter code. **d.** Structure of an *Ugi* unit along a peptoid backbone and its pendant R-groups, as well as their origin from amino acid (R_{AA}, blue), aldehyde (R_A, light blue) and isocyanate (R_{IC}, marine blue). The *Ugi*-scaffold (wine red) does not occur in the nomenclature for *Ugi* peptoid sequences. **e.** Structure of a peptide-*Ugi* peptoid hybrid and its nomenclature in letter code.

2 Experimental Section

2.1 Materials, General Methods and Instrumentation

All reagents, chemicals and solvents were purchased from commercial suppliers and used without further purification unless stated otherwise.

Nuclear Magnetic Resonance (NMR) spectra were recorded on a Bruker AV-III 400 MHz for ^{1}H and at 101 MHz for ^{13}C NMR measurements. $CDCl_3$ was used as solvent and the resonance signal at 7.26 ppm (^{1}H) and 77.16 ppm (^{13}C) served as reference for the chemical shift δ.

Gel Permeation Chromatography (GPC) measurements were conducted on an Agilent 1260 Infinity system operating in THF with 5 mM NH_4BF_4 and equipped with refractive index (RI) detector and variable wavelength detector, 2 PLgel 5 µm mixed-C columns (300 × 7.5 mm), a PLgel 5 mm guard column (50 × 7.5 mm) and an

autosampler. The instrument was calibrated with linear narrow poly(methyl methacrylate) standards in range of 550 to 46 890 g·mol^{-1}. All samples were filtered with a 0.2 µm Nylon 66 before analysis.

Matrix Assisted Laser Desorption/Ionization – Time of Flight Mass Spectroscopy (MALDI-ToF MS) was performed using a Bruker Daltonics AuToFlex MALDI-ToF mass spectrometer, equipped with a nitrogen laser at 337 nm with positive ion ToF detection. Polymer samples were measured as follows; solutions in methanol of dithranol (≥98%, Sigma Aldrich) as matrix (30 mg·mL^{-1}), silver trifluoroacetate (AgTFA) as cationization agent (10 mg·mL^{-1}) and sample (10 mg·mL^{-1}) were mixed together in a 9:1:1 volume ratio for a total volume of 75 µL. 2 µL of the mixture was applied to the target plate. Spectra were recorded in reflectron mode and the mass spectrometer was calibrated with a peptide mixture up to 6000 Da.

Reversed Phase High Performance Liquid Chromatography (RP-HPLC) on a analytical HPLC (Alliance HPLC System, Waters, UK) using a X-bridge column (C18, 3.5 µm, 4.6 × 150 mm) with a gradient of water/acetonitrile was conducted for the analysis of the oligomers.

Peptide synthesiser: The peptides were synthesized on an automated peptide synthesiser (Liberty Blue, CEN, UK) using standard 9-fluorenylmethoxycarbonyl (Fmoc) based solid phase chemistry on a 4-methylbenzhydrylamine (MBHA) *Rink* amide resin (Novabiochem, 100-200 mesh). Amino acid couplings were performed using 4 equivalents of Fmoc protected amino acids (Novabiochem), 4 eq. 1-hydroxybenzotriazole hydrate (HOBt, Carbosynth) and 4 eq. of *N*,*N'*-diisopropylcarbodiimide (DIC Alfa Aesar). Fmoc deprotections were performed with 20% piperidine in dimethylformamide.

Electrospray Ionization Mass Spectrometry (ESI-MS) were recorded at Queen Mary, University of London, on MS Agilent 6890 gc and 5973 msd (EI mode) and the LC-MS Agilent '1100 LC/MSD Trap' incorporating a SL Ion Trap. High resolution mass spectra were recorded at the National Mass Spectrometry Service, University

of Wales, Swansea, using a Thermofisher LTQ Orbitrap XL with resolution up to 100 000 Da (FWHM).

HR-ESI MS and **Tandem MS (MS/MS)** were recorded on a Q Exactive (Orbitrap) mass spectrometer (ThermoFisher Scientific, San Jose, CA, USA) equipped with an HESI II probe. The instrument was calibrated in the *m/z* range of 74-1822 using a premixed standard comprising caffeine, Met-Arg-Phe-Ala acetate (MRFA), and a mixture of fluorinated phosphazenes (Ultramark 1621). A constant spray voltage of 4.6 kV and a dimensionless sweep gas flow rate of 5 were applied. The capillary temperature and the S-lens RF level were set to 320 °C and 62.0, respectively. The samples were dissolved with a concentration of 0.05 mg·mL-1 in a mixture of THF and MeOH (3:2) containing 100 μmol sodium trifluoracetate (NaTFA). The samples were infused with a flow of 5 μL·min^{-1}.

Circular Dichroism (CD) spectra were recorded using a Chirascan spectropolarimeter (Applied Photophysics, UK) in the wavelength range 180 – 260 nm. Solutions containing 1 wt% hybrid 5 (H2O), 1 wt% Hybrid 3 dissolved in 20% MEOH, 80% H2O and 1 wt% Hybrid 8 in 10% THF and 90% H2O, were pipetted into a 0.2 mm path length, with absorbance less than 2 at any point being reported. Measurements were recorded with a 0.5 nm bandwidth, 1 mm step and 1 second collection time per point The CD signal for the background was subtracted from the CD signal of the sample, and molar ellipticity was calculated.

Cryogenic Transmission Electronic Microscopy (Cryo-TEM). Vitrified specimens were prepared using an automated FEI Vitrobot device using Quantifoil 3.5/1 holey carbon copper grids with a hole size of 3.5 µm. Before use, the grids were plasma cleaned using a Gatan Solarus 9500 plasma cleaner and then transferred into an environmental chamber of a FEI Vitrobot at room temperature and 100% humidity. Following this, the sample solution was applied onto the grid, and it was blotted twice for 5 s and then vitrified in a 1/1 mixture of liquid ethane and propane at a temperature of −180 °C. The grids with vitrified sample solution were maintained at liquid nitrogen temperature. After this, they were cryotransferred to the microscope. Imaging was carried out using a field emission cryo-electron microscope (JEOL JEM-3200FSC) operating at 200 kV. Images were taken in bright field mode and

using zero loss energy filtering (Ω type) with a slit width of 20 eV. Micrographs were recorded using a Gatan Ultrascan 4000 CCD camera. Specimen temperature was maintained at −187 °C during the imaging.

Small-angle X-ray scattering. Collection of small-angle X-ray scattering (SAXS) data was performed on the bioSAXS beamline B21, at Diamond Light Source, United Kingdom. Solutions containing 1% hybrid 5 (H2O), 1% Hybrid 3 dissolved in 20% MEOH, 80% H2O and 1% Hybrid 8 in 10% THF and 90% H2O were loaded in PCR tubes in an automated sample changer. Samples (30µl) were loaded into a temperature controlled quartz cell capillary and exposed for 10 seconds, 18 frames at 15oC. Data was collected using a dectris pilatus 2m detector. Background was manually subtracted using SCATTER . Form factor modelling was done using SASFIT.

2.2 Synthesis of Monomers

2.2.1 Synthesis of Polystyrene Butyl Amine Resin

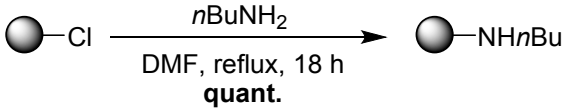

To a suspension of crosslinked (chloromethyl)polystyrene (5.5 mmol/g Cl loading, 10.0 g, 55.0 mmol) and DMF (40 mL) *n*butylamine (20.1 g, 275 mmol) was added and the mixture was stirred under reflux over night. The polystyrene butyl amine resin was filtered off and washed with DCM (250 mL), dried under vacuum and used as obtained.

2.2.2 Synthesis of (2*R*,4*S*,5*R*)-2-(acetoxymethyl)-6-((3-oxopropyl)thio)tetrahydro-2*H*-pyran-3,4,5-triyl triacetate

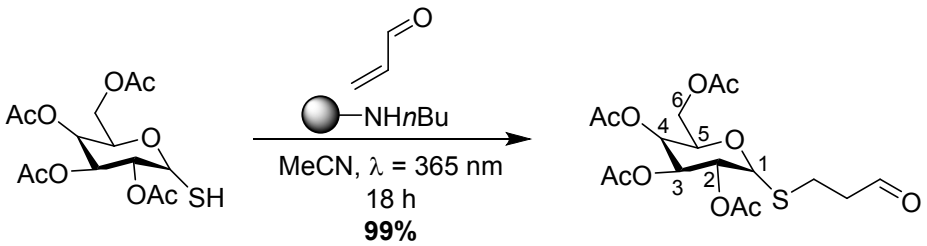

(2*R*,4*S*,5*R*)-2-(acetoxymethyl)-6-mercaptotetrahydro-2*H*-pyran-3,4,5-triyl triacetate (525 mg, 1.44 mmol) was dissolved in MeCN (1.5 mL) and the

polystyrene butyl amine resin (131 mg, 720 μmol) was added. Acrolein (162 mg, 2.88 mmol) was added and the suspension was stirred under UV light radiation (λ = 365 nm) over night. The solid phase was filtered off and the solvent was removed under reduced pressure to obtain a sticky, colourless oil (655 mg, >99%).

^{1}H NMR ($CDCl_3$, 400 MHz) δ (ppm) = 9.77 (d, *J* = 1.0 Hz, 1H, C*H*O), 5.22 (t, *J* = 9.4 Hz, 1H, C^3H), 5.10 – 4.99 (2 t, 2H, *J* = 9.8 Hz, C^2H and *J* = 9.3 Hz, C^4H), 4.52 (d, *J* = 10.0 Hz, 1H, C^1H), 4.22 (dd, J = 12.4, 4.9 Hz, 1H, CHC^6H_2OAc), 4.15 (dd, *J* = 12.4, 2.4 Hz, 1H, $CHCH_2OAc$), 3.70 (ddd, *J* = 10.1, 4.9, 2.4 Hz, 1H), 3.03 – 2.88 (m, 2H, SCH_2CH_2), 2.88 – 2.76 (m, 2H, CH_2CH_2CHO), 2.10 – 1.99 (4 s, 12H, $COCH_3$).

^{13}C NMR ($CDCl_3$, 400 MHz) δ (ppm) = 200.1 (*C*HO), 170.7 (*C*OOAc), 170.3 (*C*OOAc), 169.6 (*C*OOAc), 169.5(*C*OOAc), 83.8 (C^1), 76.1 (C^5), 73.9 (C^3), 69.8 (C^4), 68.4 (C^2), 62.1 (C^6), 44.6 (CH_2CH_2CHO), 22.4 (SCH_2CH_2), 20.9 ($COOCH_3$), 20.8 ($COOCH_3$), 20.7 ($COOCH_3$), 20.7 ($COOCH_3$).

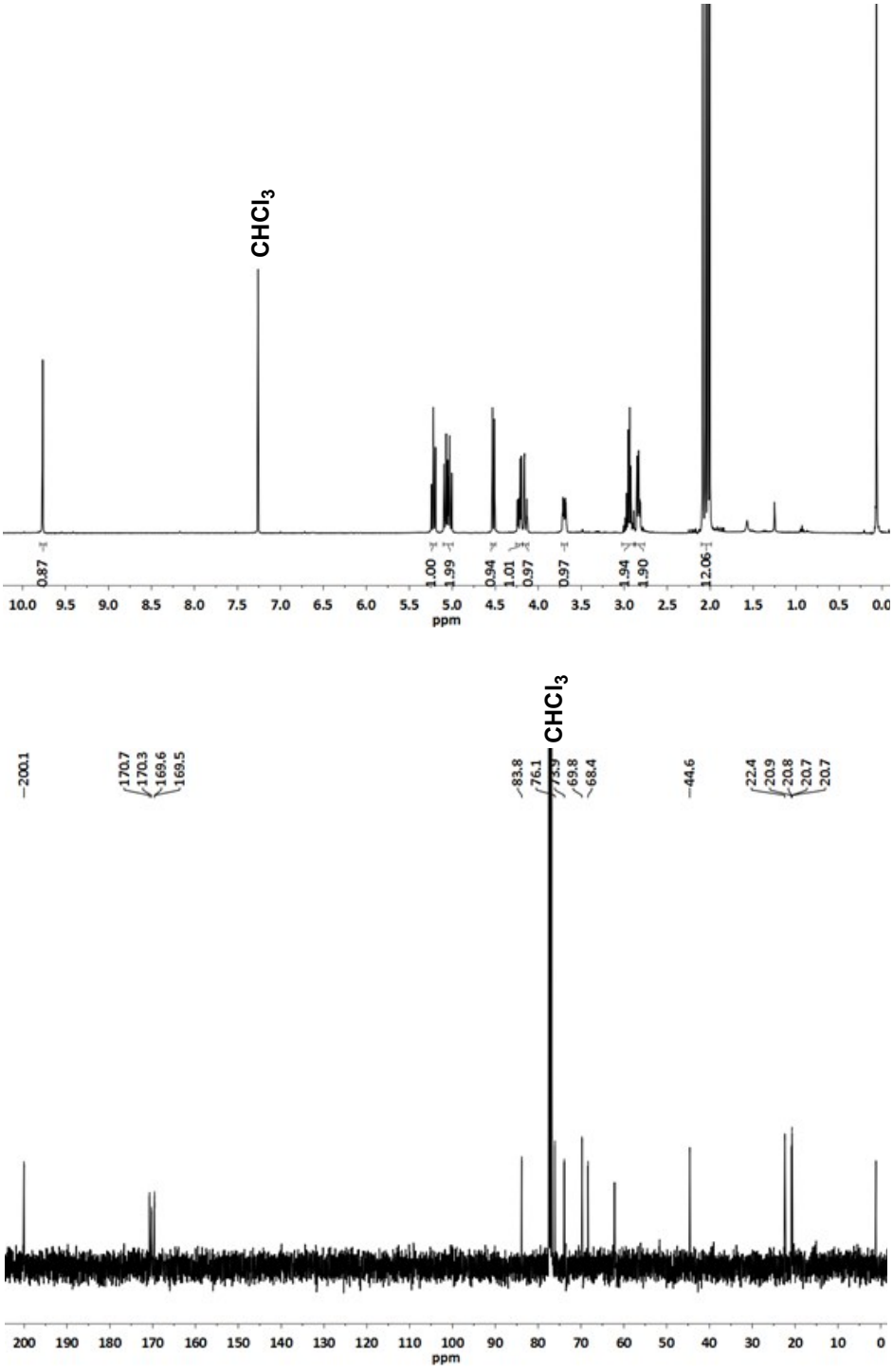

Figure S2 | NMR analysis of (2*R*,4*S*,5*R*)-2-(acetoxymethyl)-6-((3-oxopropyl)thio) tetrahydro-2*H*-pyran-3,4,5-triyl triacetate. Top: ^{1}H NMR analysis in $CDCl_3$; **bottom:** ^{13}C NMR analysis in $CDCl_3$.

2.2.3 Synthesis of MeO-PEG$_{550}$-CHO

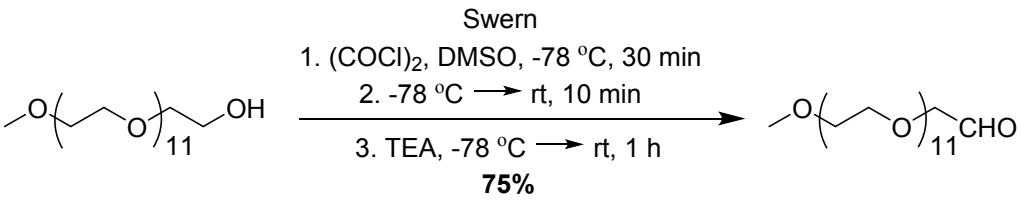

Oxalylchloride (1.00 g, 7.88 mmol) and dry DCM (30 mL) were cooled to –78 °C. DMSO (3 mL) was added and the reaction mixture was stirred at –78 °C for 30 min. PEG methyl ether (M_n = 500 g/mol, 2.63 g, 5.25 mmol) was added and the reaction mixture was stirred at –78 °C for 30 min. The mixture was warmed slowly until the PEG methyl ether was dissolved and it was cooled again to –78 °C. Triethylamine (7 mL) was added dropwise and it was stirred at constant temperature for 1 h. After warming to room temperature, the solvent was removed under reduced pressure. Chloroform (20 mL) and water (20 mL) and the phases were separated. The combined organic layers were dried over $MgSO_4$ and the solvent was evaporated. A yellow oil was obtained (1.98 g, 75%).

^{1}H NMR ($CDCl_3$, 400 MHz) δ (ppm) = 9.54 (s, 1H, C*H*O), 4.00 (s, 2H, OCH_2CHO), 3.59 – 3.32 (m, 55H, -CH_2-), 3.19 (s, 3H, OCH_3).

^{13}C NMR ($CDCl_3$, 400 MHz) δ (ppm) = 200.4 (*C*HO), 76.4 (O*C*H_2CHO), 71.4 (-*C*H_2-), 70.7 (-*C*H_2-), 70.3 (-*C*H_2-), 70.2 (-*C*H_2-), 70.1(-*C*H_2-), 70.0 (-*C*H_2-), 58.5 (O*C*H_3).

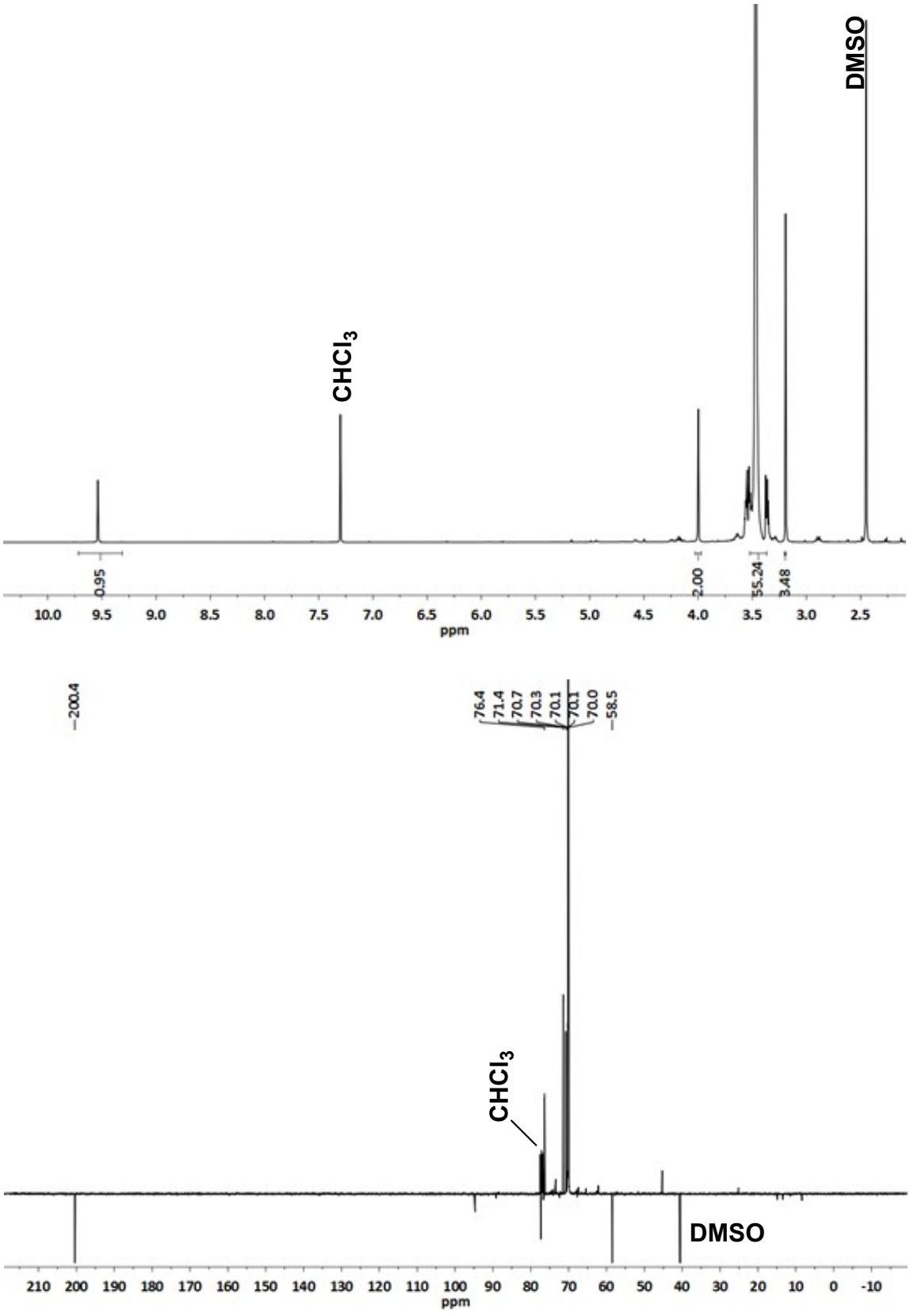

Figure S3 | NMR analysis of MeO-PEG$_{550}$-CHO. Top: ^{1}H NMR analysis in $CDCl_3$; **bottom:** ^{13}C NMR analysis in $CDCl_3$.

MALDI-ToF Analysis:

MeO-PEG$_{550}$-OH:

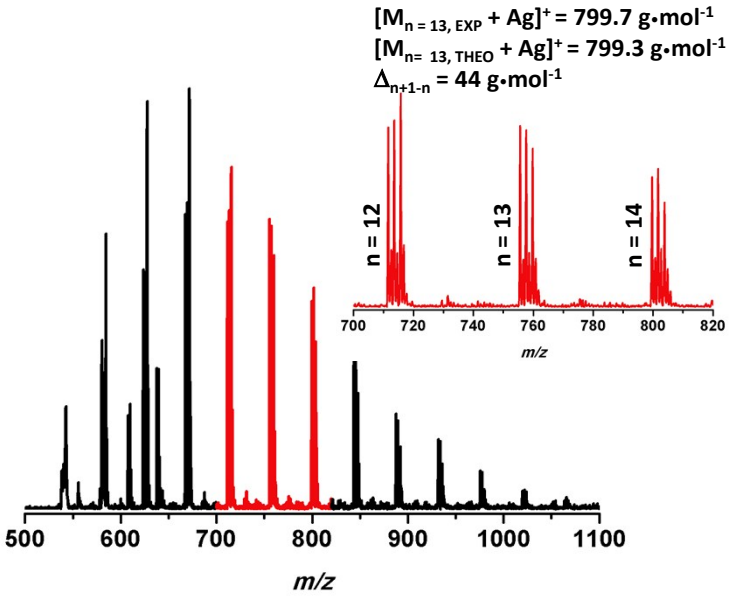

MeO-PEG$_{550}$-CHO:

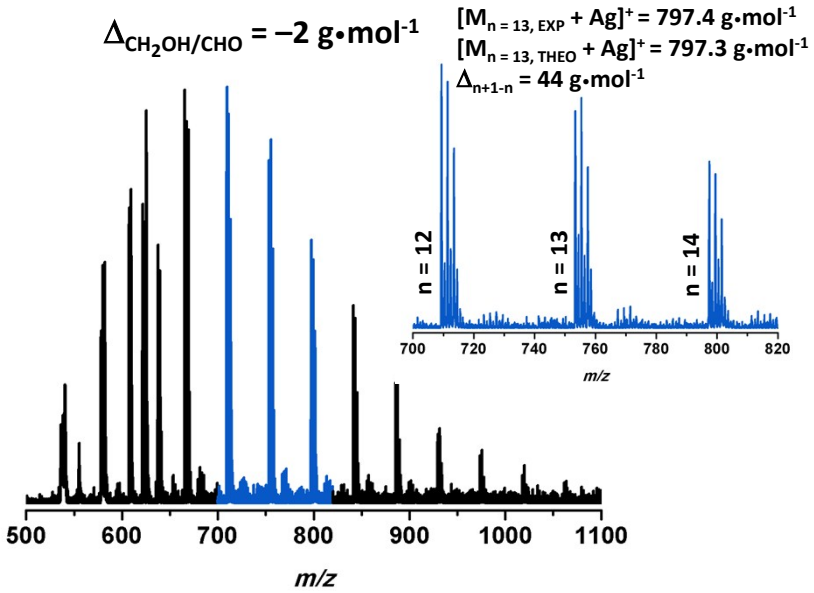

Figure S4 | MALDI-ToF analysis of MeO-PEG$_{550}$-OH and MeO-PEG$_{550}$-CHO.

3 Synthesis and Characterisation of Oligomers

3.1 General Procedures

(1) Automated Deprotection of the resin. After swelling in $CHCl_3$, the Fmoc-Rink amide was deprotected with DMF/piperidine 3/1 *v/v* (20 mL) solution under microwave irradiation (125 W) at 75 °C for 30 sec and the second under the same conditions during 180 sec.

(2) Automated Fmoc-Solid Phase Peptide Synthesis (Fmoc-SPPS) of the anchors. H_2N-FGF-$CONH_2$ and H_2N-KKKK-$CONH_2$ peptide anchor was synthesised on Fmoc-Rink amide (0.78 mmol/g, 1.00 eq) resin following the automated Fmoc strategy of solid phase peptide synthesis. The Fmoc protected amino acids (4.00 eq), the coupling reagent (4.00 eq) and DIC (4.00 eq) were added to the vessel containing the deprotected resin and the mixture was stirred using nitrogen flux under microwave irradiation (45 W) at 75 °C for 600 sec. After each coupling reaction, the resin was submitted to two deprotection cycles as reported in *(1)*.

(3) Manual Fmoc-Solid Phase Peptide Synthesis (Fmoc-SPPS). Peptide units were synthesised on resin following the conventional Fmoc strategy of solid phase peptide synthesis. The Fmoc protected amino acids (4.00 eq), HOBt (4.00 eq) and DIC (4.00 eq) were added to the vessel containing the deprotected resin and the mixture was stirred in DMF at 40 °C for 2 h. The resin was washed with 2 x DCM (10 mL) and 2 x DMF (10 mL). After each coupling reaction, two deprotection cycles using DMF/piperidine 3/1 *v/v* (12 mL) were conducted and the resin was washed with 3 x MeOH/$CHCl_3$ 1/3 *v/v* (10 mL). Kaiser test was conducted to determine the success of the reaction.

(4) Manual Ugi-Fmoc-Solid Phase Peptoid Synthesis (Ugi-Fmoc-SPPS). Peptoid units were synthesised on resin following *Ugi*-Fmoc strategy of solid phase peptoid synthesis. The deprotected resin and aldehyde (4.00 eq) were stirred in the minimal amount of MeOH/$CHCl_3$ 3/1 *v/v* (10 mL) at 60 °C for 30-60 min in order to ensure the imine formation. Fmoc protected amino acids (5.00 eq) and isocyanide (6.00 eq) were added and the reaction was stirred at 60 °C for 2-6 h. The resin was washed with 2 x DCM (10 mL) and 2 x DMF (10 mL). After each *Ugi* reaction, two deprotection cycles using DMF/piperidine 3/1 *v/v* (12 mL) were conducted and the

resin was washed with with 3 x DCM (10 mL), when peptide coupling was following, or 3 x MeOH/$CHCl_3$ 3/1 *v/v* (10 mL), when Ugi reaction was following.

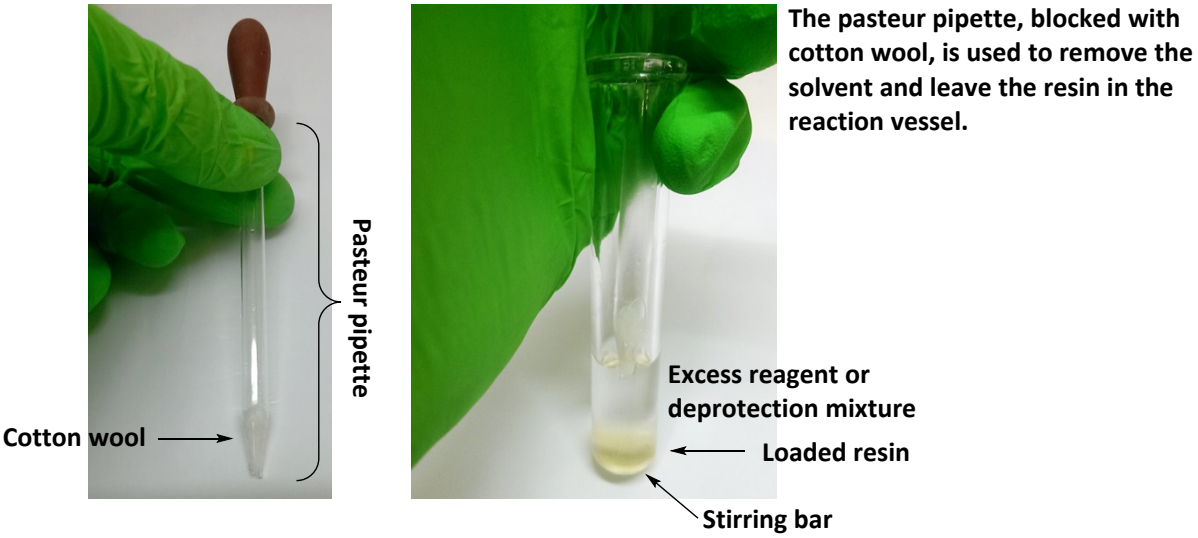

Figure S5 | Benchtop solid phase. The reaction vessel is charged with the loaded resin and a stirring bar and can be heated in an oil bath at the desired temperature. After the coupling or deprotection reaction, the solution phase containing excess or deprotection reagents is removed *via* inverted filtration, whereby the resin remains in the vessel. This method was employed for (*3*) Fmoc-SPPS and (*4*) *Ugi*-Fmoc-SPPS.

(5) Cleavage. Oligomers were cleaved from resin in neat DCM/trifluoroacetic acid 1/1 *v/v* (15 mL) for 2 h. After removal of the resin by filtration, the solution was concentrated by bubbling heavily with air. Water was added and the crude product mixture was lyophilized.

(6) Purification. The mixture was either dissolved in MeOH (2 mL) and precipitated in cold Et_2O (25 mL) or treated with Et_2O (5 mL). The precipitate was separated *via* decantation or filtration and analysed as obtained.

3.2 Characterisation of Oligomers

3.2.1 Characterisation of H_2N-F(*n*Pr,Cy)-F-G-F-$CONH_2$ 1:

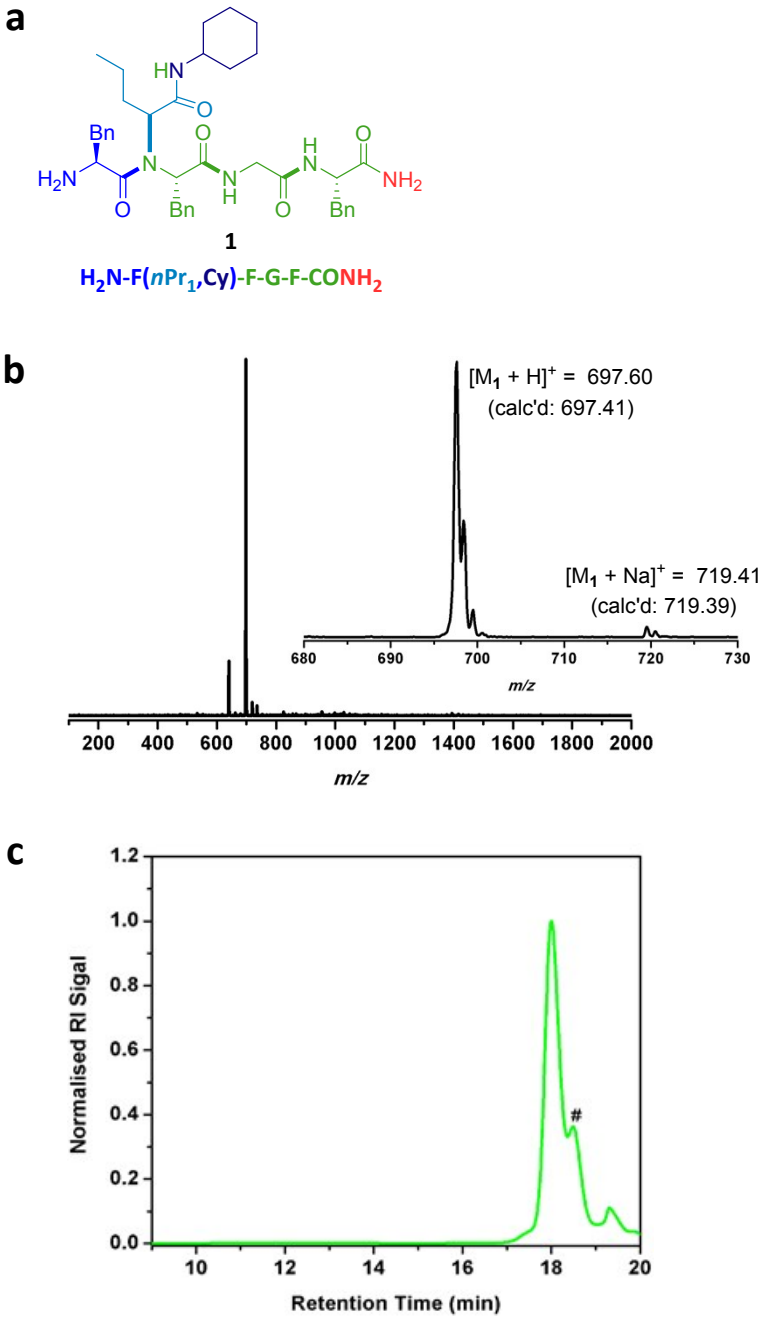

Figure S6 | Structure and characterisation of 1. a. Structure of compound **1**. **b.** Positive ESI-MS analysis of crude **1** after cleavage. **c.** SEC traces of **1** after cleavage obtained in DMF at 25 °C (# = not identified impurity).

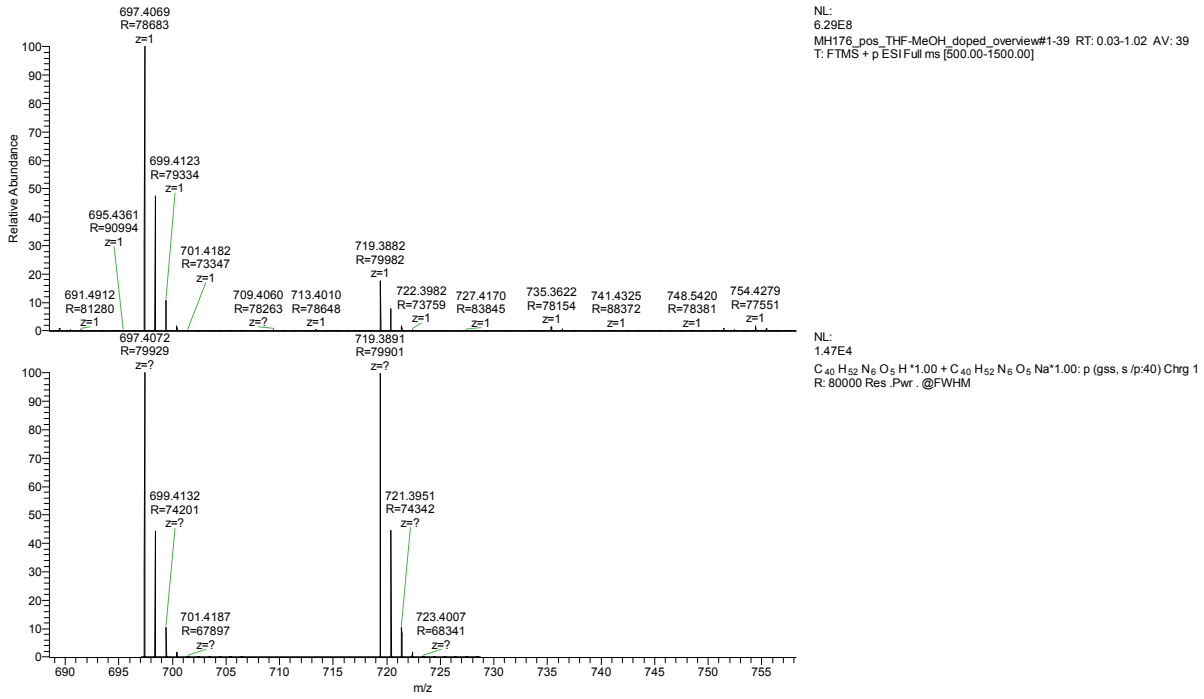

Peak	m/z exp	m/z theo	resolution	Δm
$[M + H]^+$	697.4069	697.4072	79 000	0.0003
$[M + Na]^+$	719.3882	719.3891	80 000	0.0009

Figure S7 | HR-ESI MS of 1. top. Experimental spectra of **1**. **top.** Theoretical spectra of **1**. **Bottom**.

3.2.2 Characterisation of H_2N-F($C_{10}H_{21}$,Cy)-F-G-F-$CONH_2$ 2:

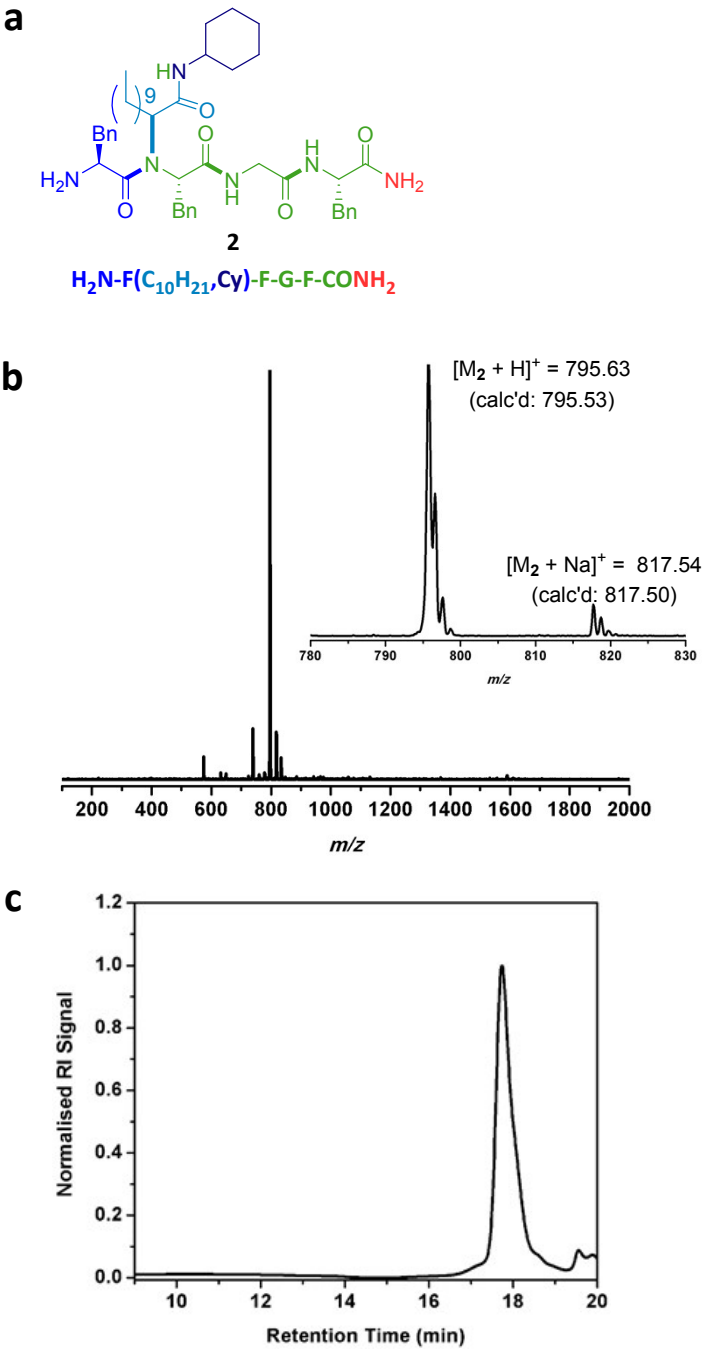

Figure S8 | Structure and characterisation of 2. a. Structure of compound **2**. **b.** Positive ESI-MS analysis of crude **2** after cleavage. **c.** SEC traces of **2** after cleavage obtained in DMF at 25 °C (*Đ* = 1.04).

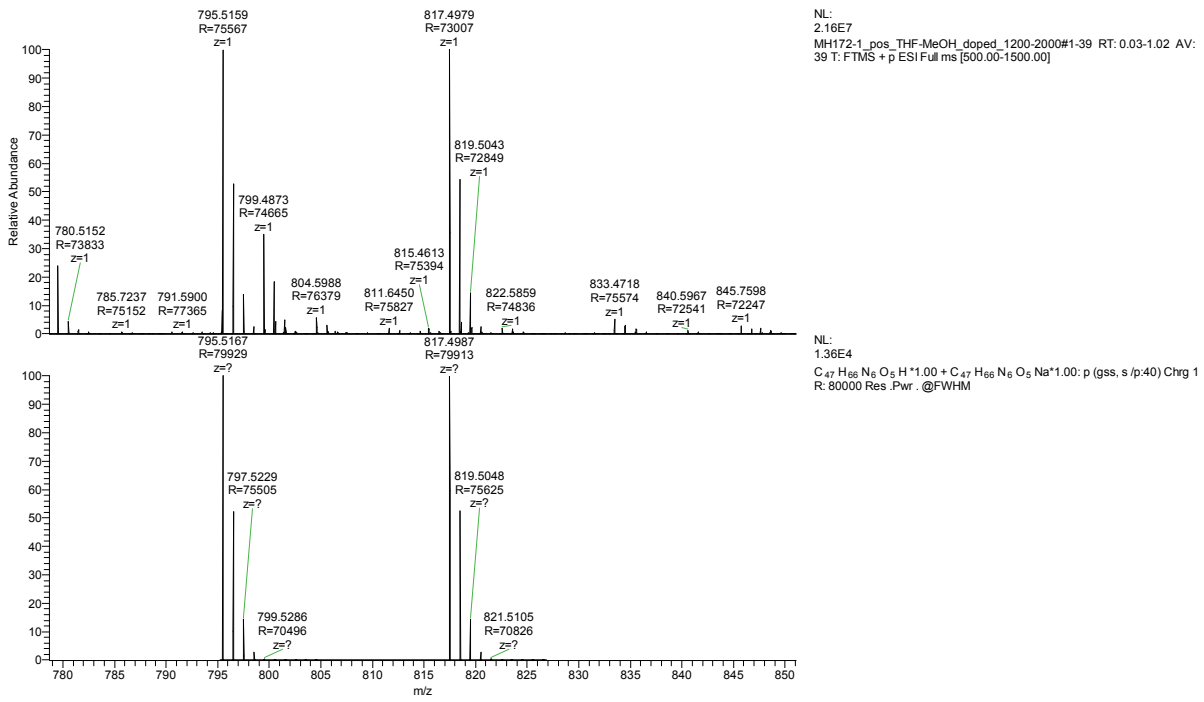

Peak	m/z exp	m/z theo	resolution	Δm
$[M + H]^+$	795.5159	795.5167	76 000	0.0008
$[M + Na]^+$	817.4979	817.4987	73 000	0.0008

Figure S9 | HR-ESI MS of 2. top. Experimental spectra of **2**. **top.** Theoretical spectra of **2**. **bottom**.

3.2.3 Characterisation of H_2N-F-F(*n*Pr,Cy)-K-K-K-K-$CONH_2$ 3:

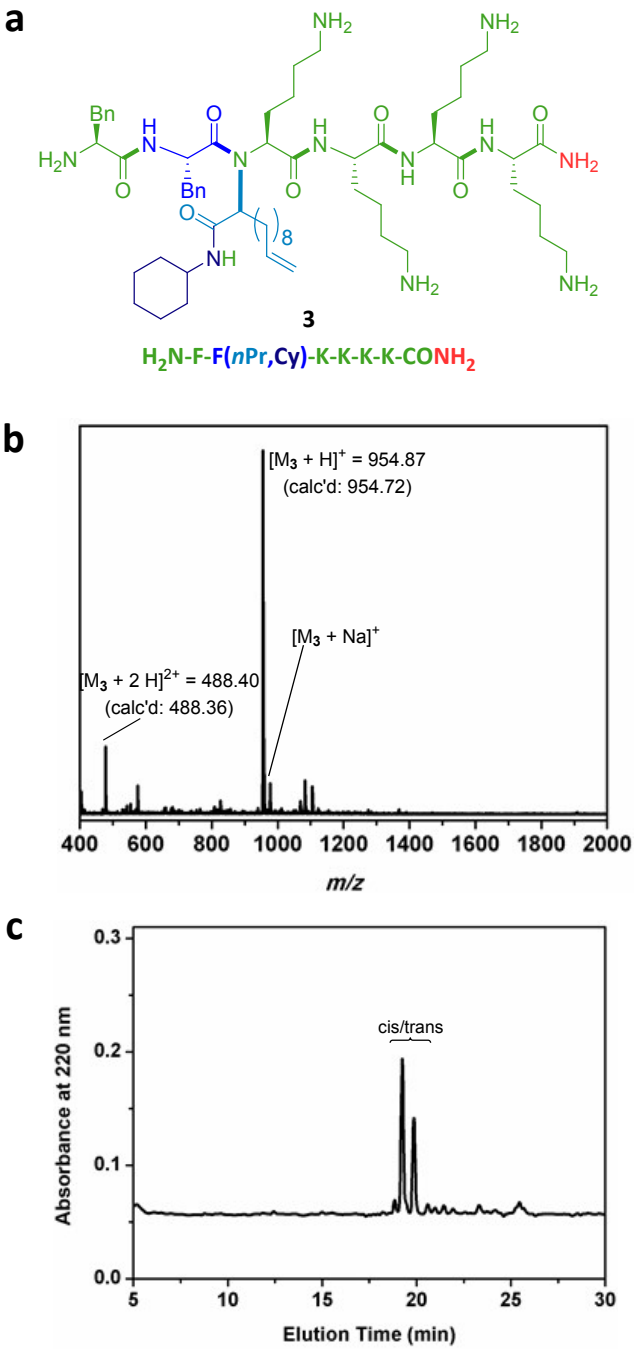

Figure S10 | Structure and characterisation of 3. a. Structure of compound **3**. **b.** Positive ESI-MS analysis of crude **3** after cleavage. **c.** RP-HPLC traces recorded for oligomer **3** after cleavage (54% purity). The analysis was performed with a linear gradient of 98 to 2% water in 20 min using water/MeCN as mobile phase with 0.1% TFA.

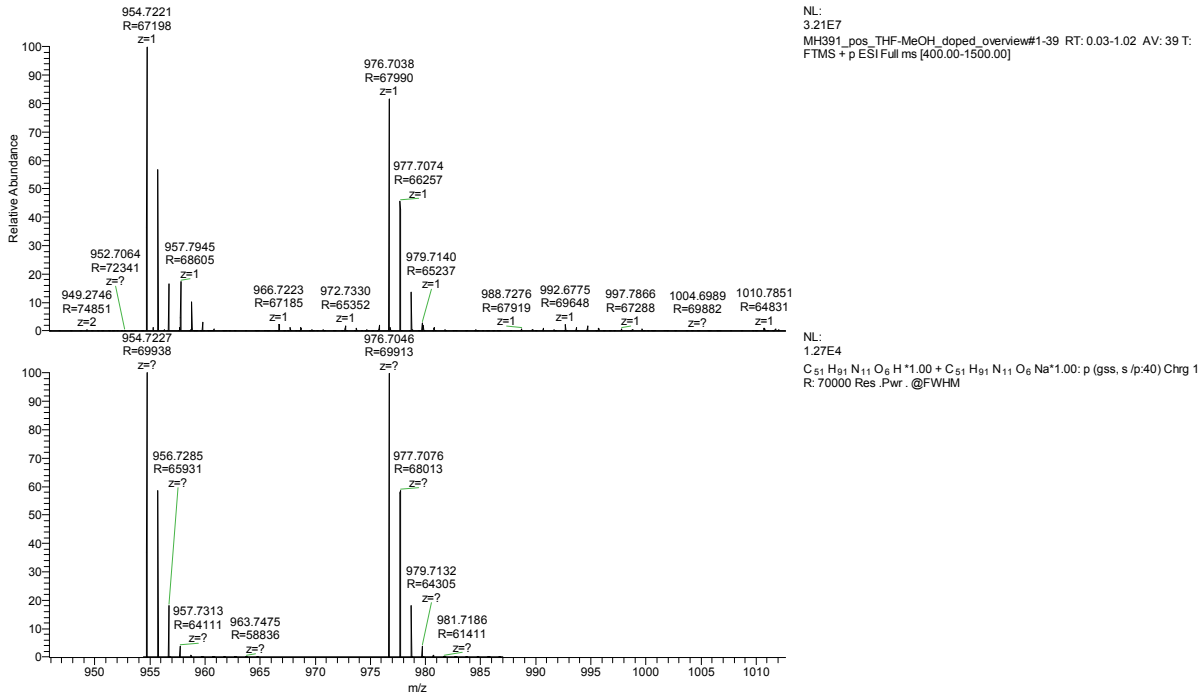

Peak	m/z exp	m/z theo	resolution	Δm
$[M + H]^+$	954.7221	954.7227	67 000	0.0006
$[M + Na]^+$	976.7038	976.7046	68 000	0.0008

Figure S11 | HR-ESI MS of 3. top. Experimental spectra of **3**. **top.** Theoretical spectra of **3**. **bottom.**

3.2.4 Characterisation of H_2N-F-F(*n*Pr,Cy)-K-K-K-K-$CONH_2$ 4:

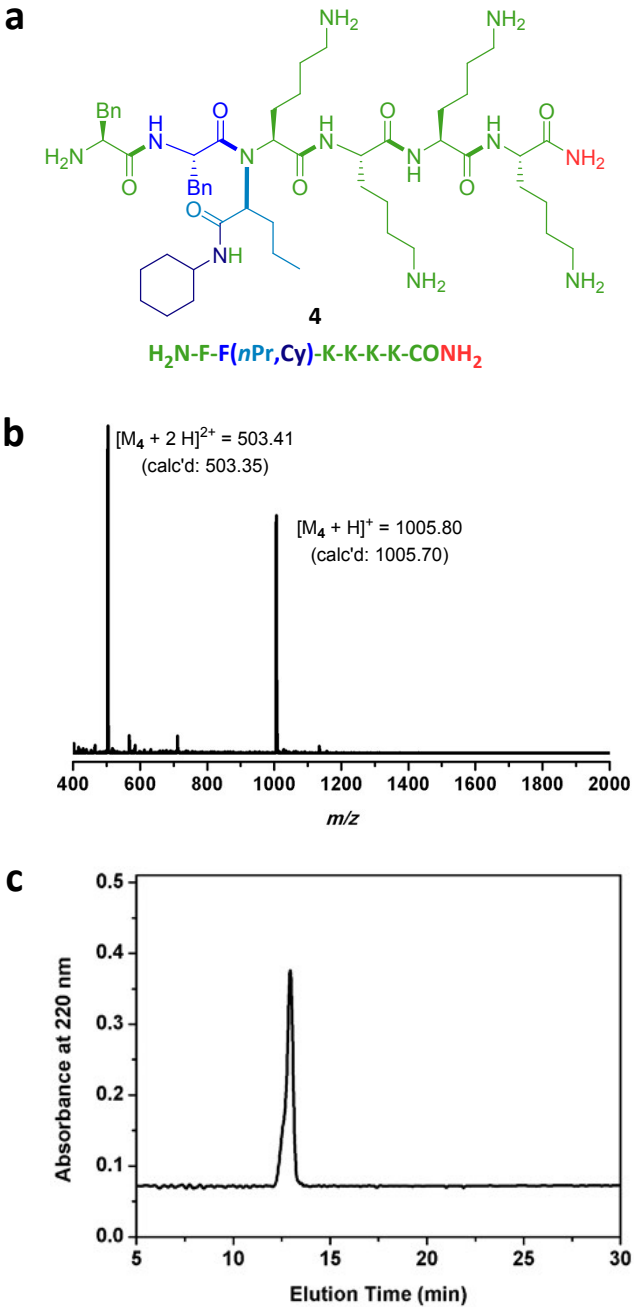

Figure S12 | Structure and characterisation of 4. a. Structure of compound **4**. **b.** Positive ESI-MS analysis of crude **4** after cleavage. **c.** RP-HPLC traces recorded for oligomer **4** after cleavage (>99% purity). The analysis was performed with a linear gradient of 98 to 2% water in 20 min using water/MeCN as mobile phase with 0.1% TFA.

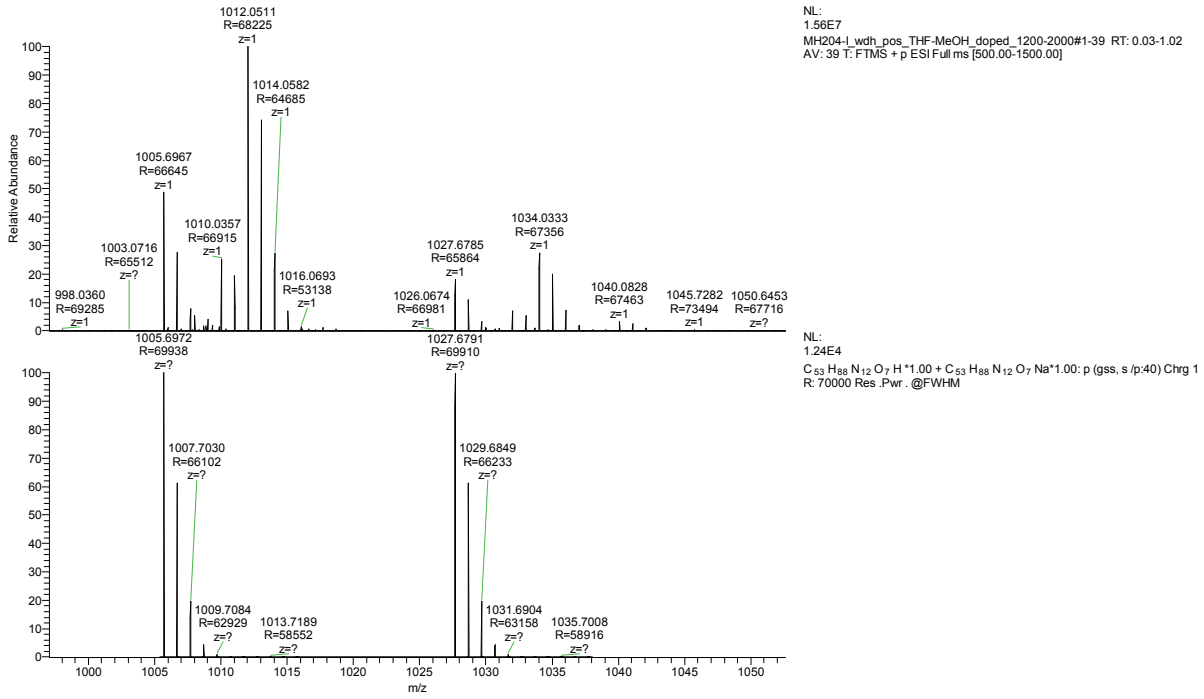

Peak	m/z exp	m/z theo	resolution	Δm
$[M + H]^+$	1005.6967	1005.6972	68 000	0.0005
$[M + Na]^+$	1027.6785	1027.6791	66 000	0.0006

Figure S13 | HR-ESI MS of 4. top. Experimental spectra of **4**. **top.** Theoretical spectra of **4**. **bottom.**

3.2.5 Characterisation of H_2N-F$(CH_2)_2$-S-Glu(OAc_4),Cy)-K-K-K-K-$CONH_2$ 5:

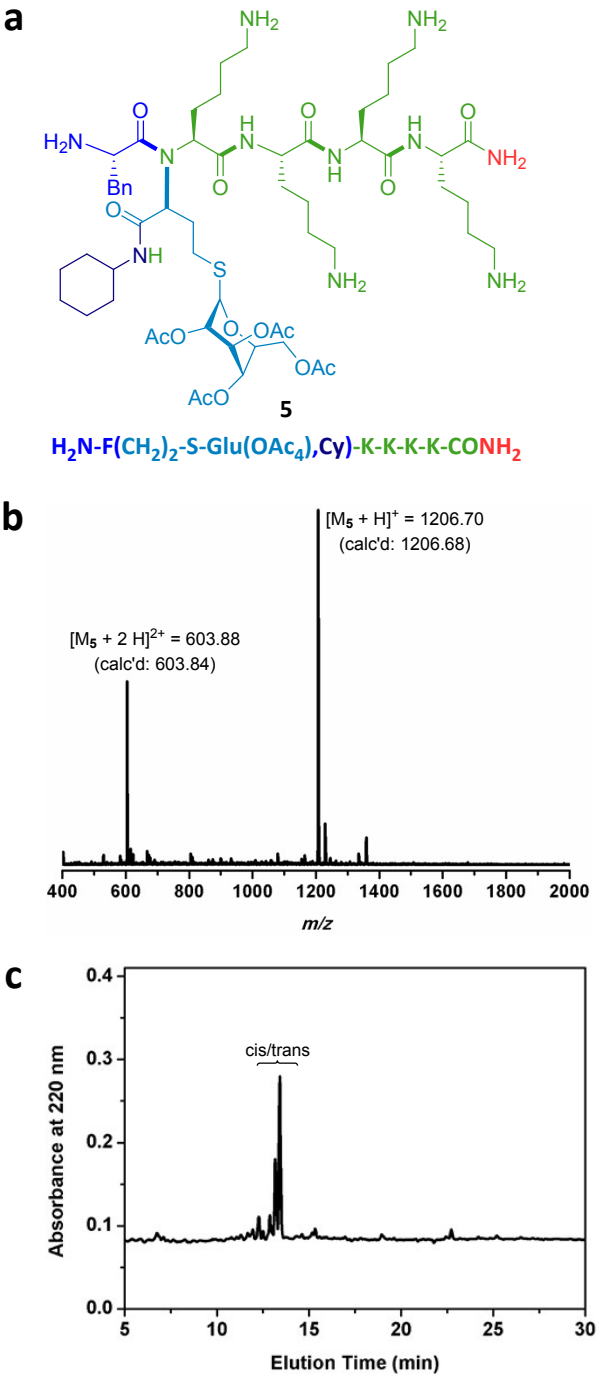

Figure S14 | Structure and characterisation of 5. a. Structure of compound **X**. **b.** Positive ESI-MS analysis of crude **5** after cleavage. **c.** RP-HPLC traces recorded for oligomer **5** after cleavage (99% purity). The analysis was performed with a linear gradient of 98 to 2% water in 20 min using water/MeCN as mobile phase with 0.1% TFA.

3.2.6 Characterisation of Fmoc-F(PEG$_{550}$,Cy)-K-K-K-K-CONH$_2$ 6:

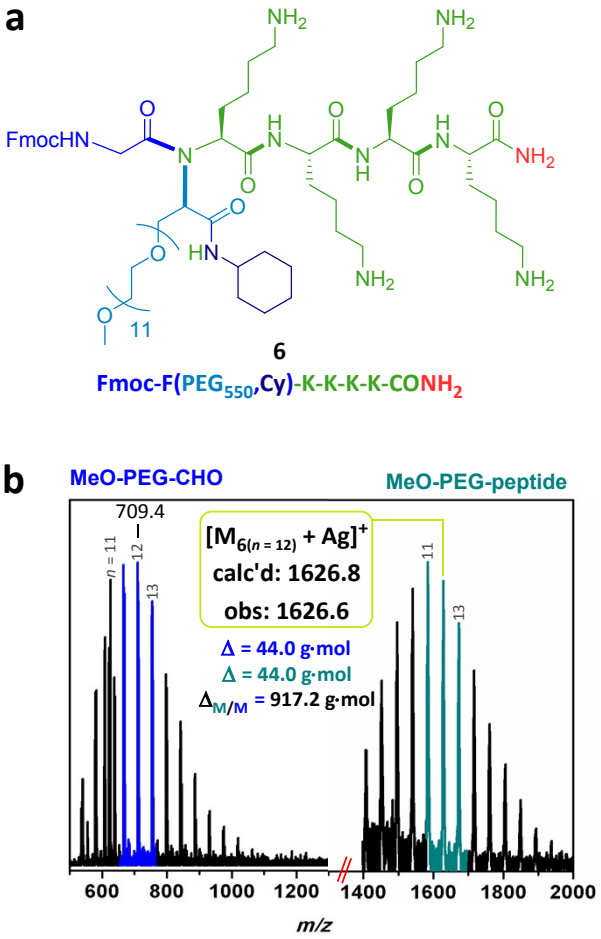

Figure S15 | Structure and characterisation of 6. a. Structure of compound **6**. **b.** MALDI-ToF analysis of crude **6** after cleavage using dithranol as matrix and Ag^+TFA^- as polarising agent.

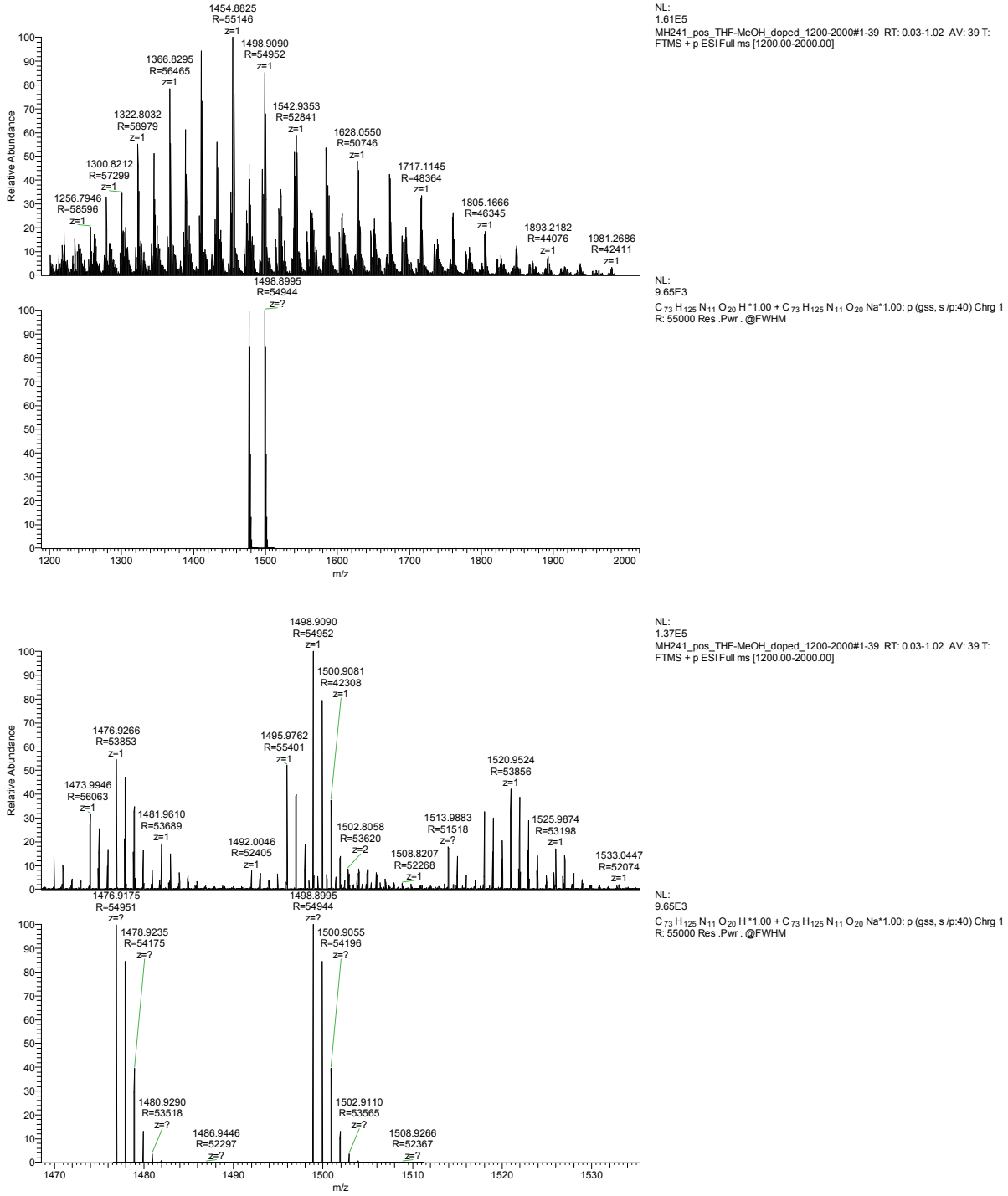

Peak	m/z exp	m/z theo	resolution	Δm
$[M_{n=11} + H]^+$	1476.9266	1476.9175	54 000	0.0091
$[M_{n=11} + Na]^+$	1498.9090	1498.8995	55 000	0.0095

Figure S16 | HR-ESI MS of 6. top. Experimental spectra of **6**. **middle.** Theoretical spectra of **6**. **bottom.**

3.2.7 Characterisation of H_2N-F($C_{10}H_{21}$,Cy)-F-F(*n*Pr,Cy)-F-F($C_{10}H_{21}$,Cy)-F-G-F-$CONH_2$ 7:

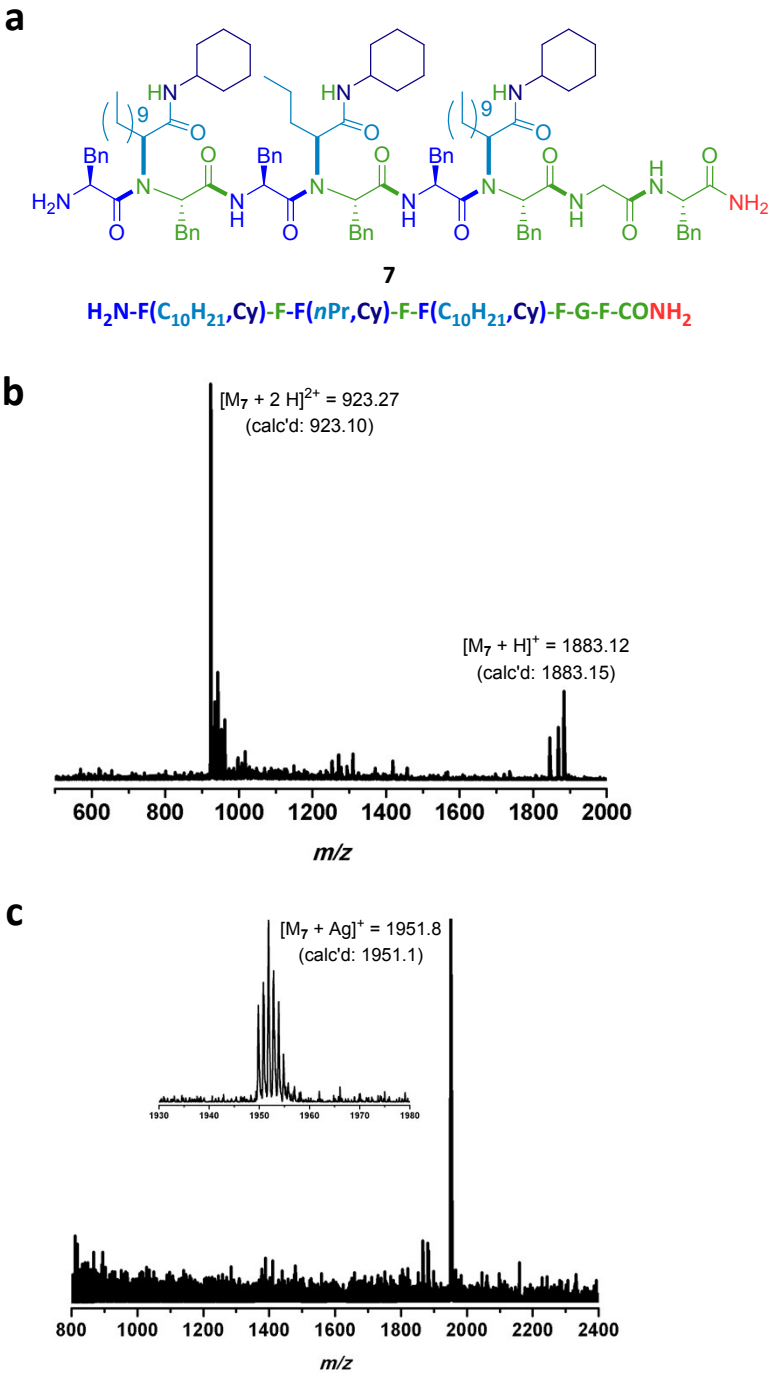

Figure S17 | Structure and characterisation of 7. a. Structure of compound **7**. **b.** Positive ESI-MS analysis of crude **7** after cleavage. **c.** MALDI-ToF analysis of crude **5** after cleavage using dithranol as matrix and Ag^+TFA^- as polarising agent.

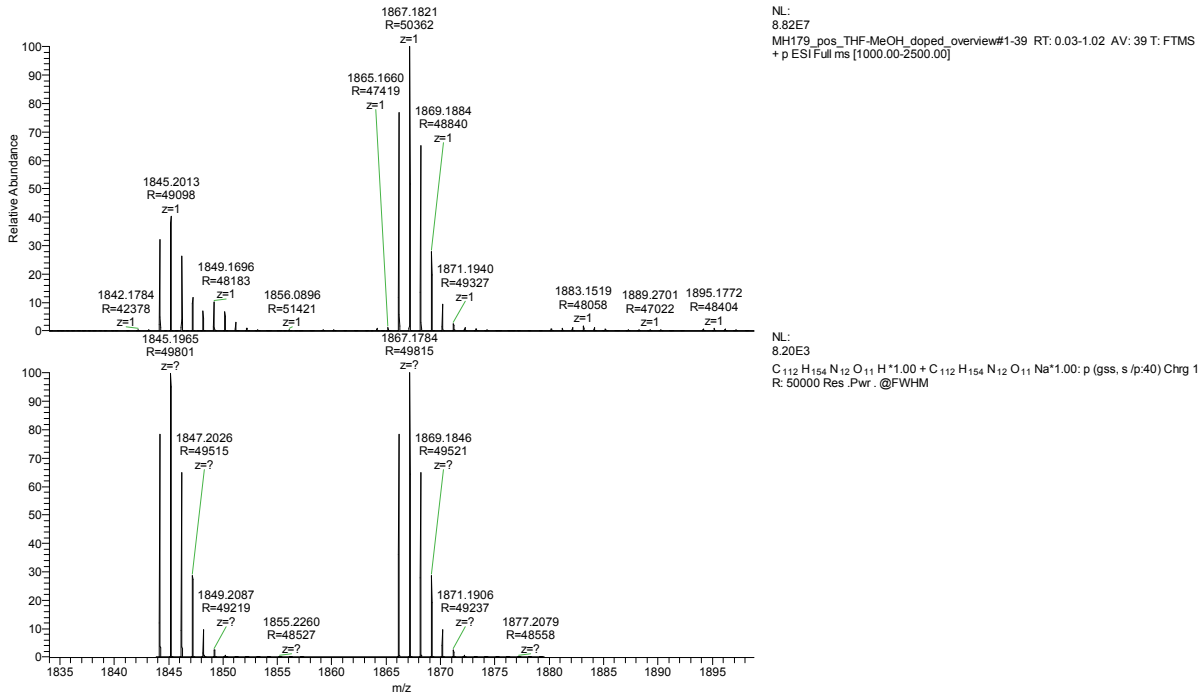

Peak	m/z exp	m/z theo	resolution	Δm
$[M + H]^+$	1845.2013	1845.1965	49 000	0.0048
$[M + Na]^+$	1867.1821	1867.1784	50 000	0.0037

Figure S18 | HR-ESI MS of 7. top. Experimental spectra of **7**. **top.** Theoretical spectra of **7**. **bottom.**

3.2.8 Characterisation of Fmoc-F(*n*Pr,Cy)-F-F(*n*Pr,Cy)-F-F(*n*Pr,Cy)-K-K-K-K-$CONH_2$ 8:

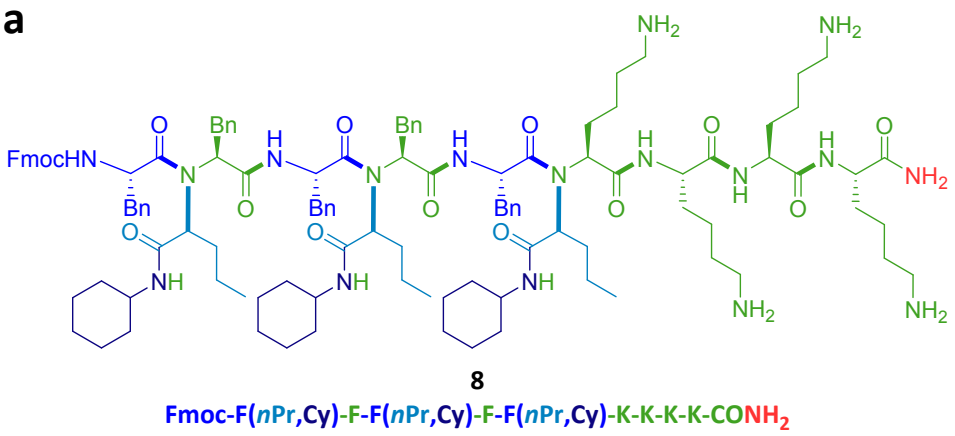

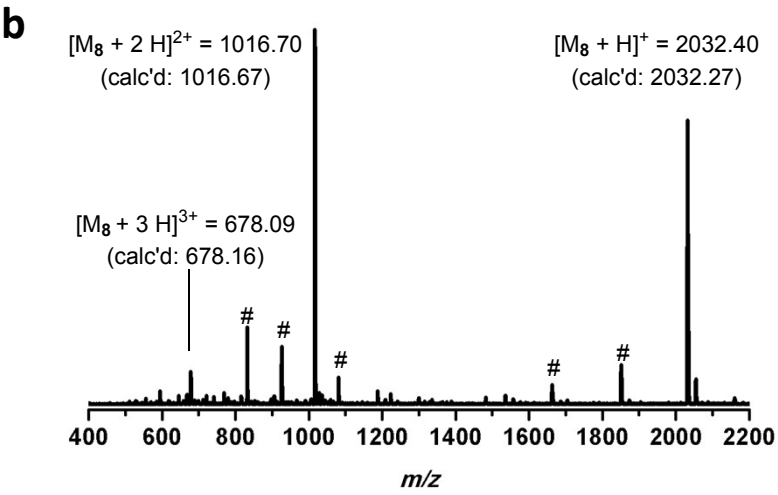

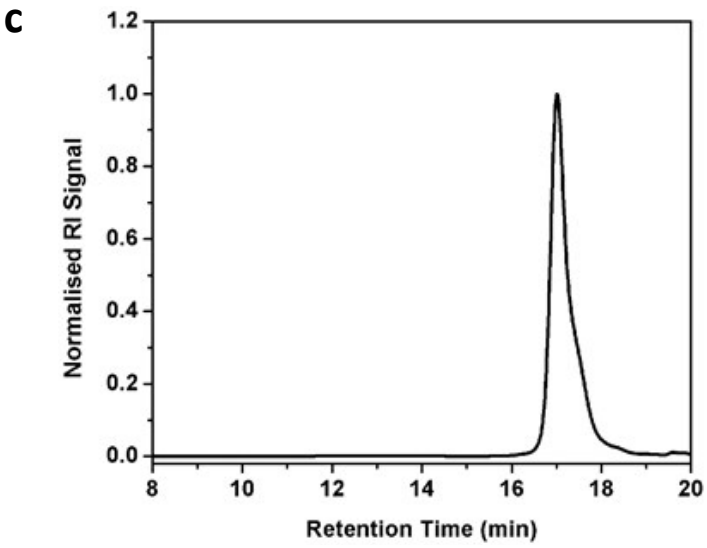

Figure S19 | Structure and characterisation of 8. a. Structure of compound **8**. **b.** Positive ESI-MS analysis of crude **8** after cleavage (# = not identified impurities). **c.** SEC traces of **8** after cleavage obtained in DMF at 25 °C (*Đ* = 1.09).

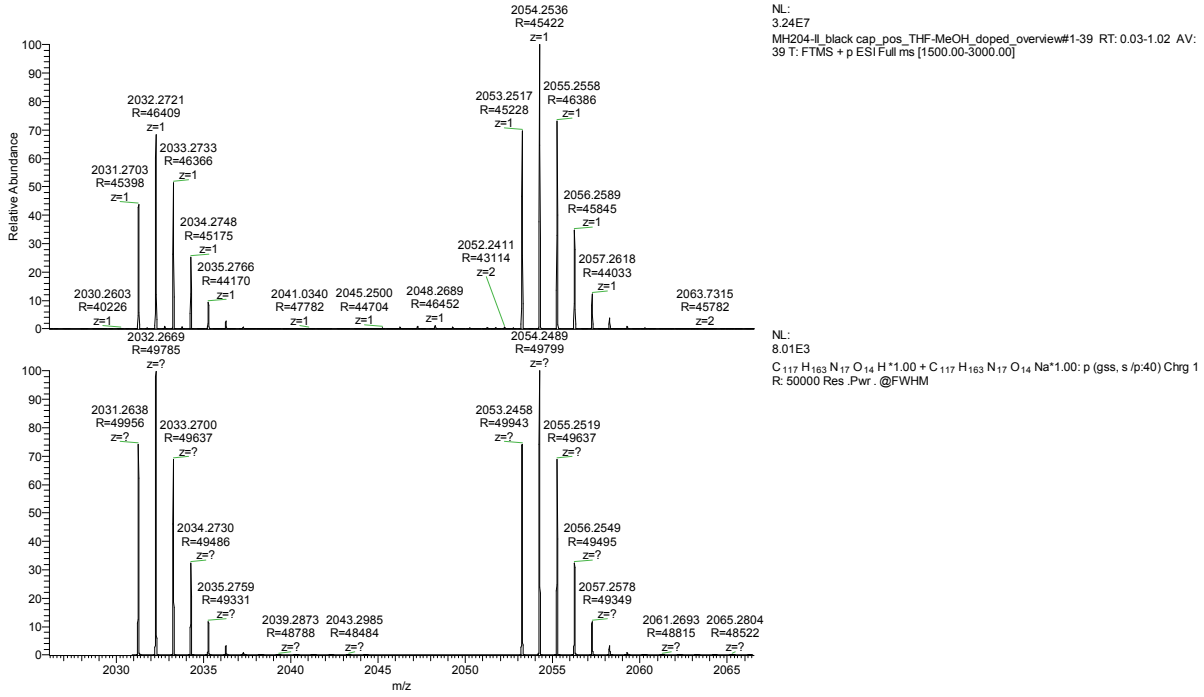

Peak	m/z exp	m/z theo	resolution	Δm
$[M + H]^+$	2031.2703	2031.2638	45 000	0.0065
$[M + Na]^+$	2053.2517	2053.2458	45 000	0.0059

Figure S20 | HR-ESI MS of 8. top. Experimental spectra of **8**. **top.** Theoretical spectra of **8**. **bottom.**

3.2.9 Characterisation of H_2N-K(CH_2)$_2$-S-Glu),Cy)-K(CH_2)$_2$-S-Glu),Cy)-K(CH_2)$_2$-S-Glu),Cy)-K-K-K-K-$CONH_2$ 9:

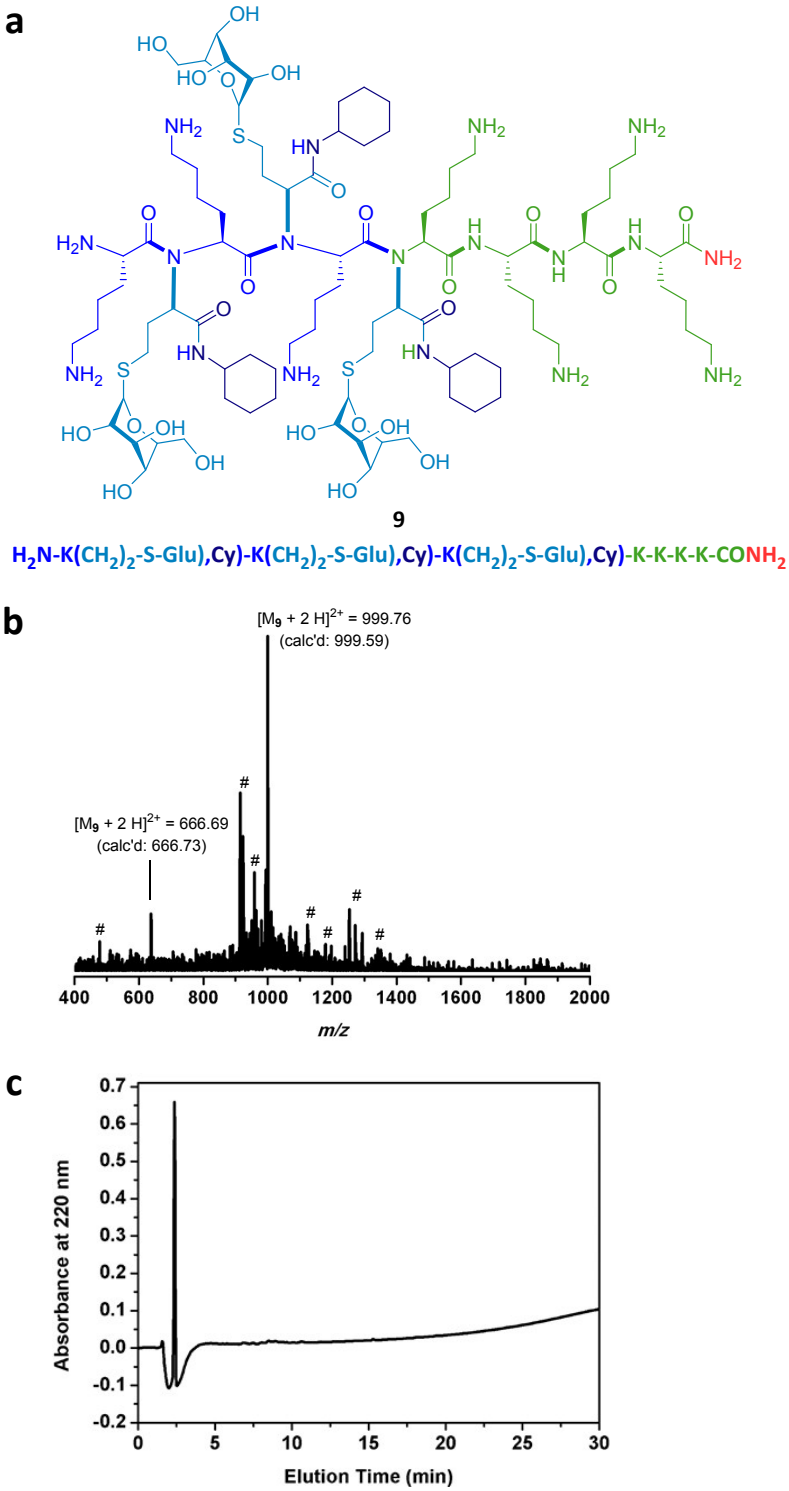

Figure S21 | Structure and characterisation of 9. a. Structure of compound **9**. **b.** Positive ESI-MS analysis of crude **9** after cleavage. **c.** RP-HPLC traces recorded for oligomer **9** after cleavage (99% purity). The analysis was performed with a linear gradient of 98 to 2% water in 20 min using water/MeCN as mobile phase with 0.1% TFA.

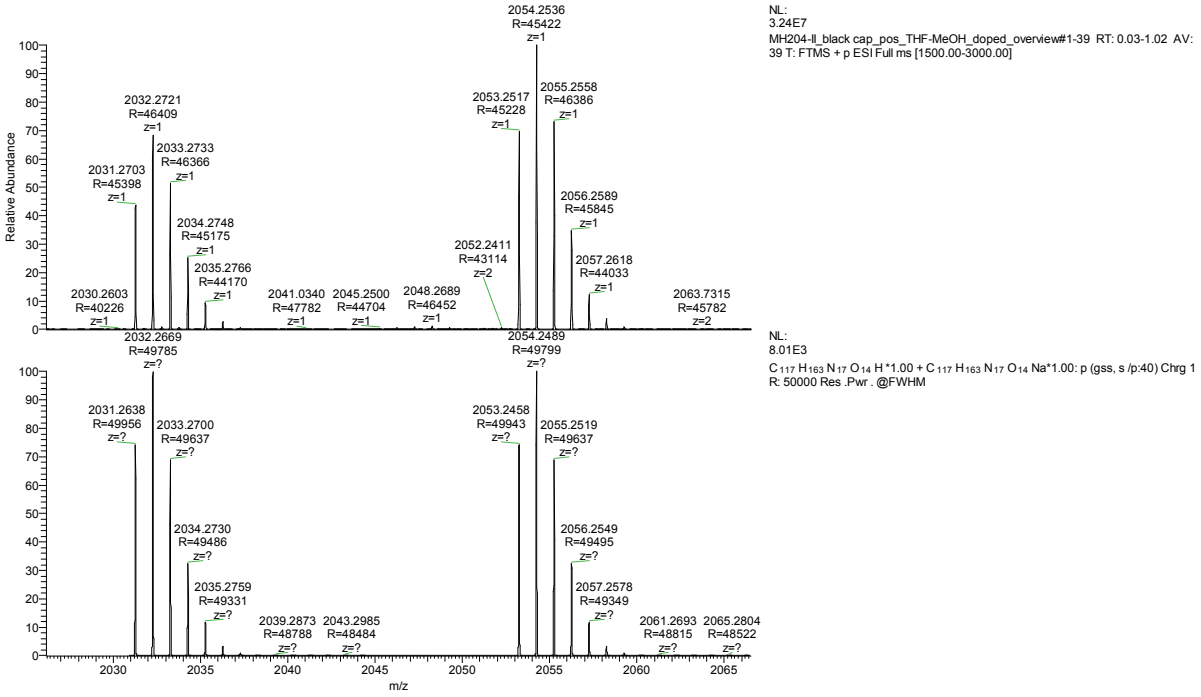

Peak	m/z exp	m/z theo	resolution	Δm
$[M + H]^+$	1999.1851	1999.1692	48 000	0.0159
$[M + Na]^+$	2021.1673	2021.1512	47 000	0.0161

Figure S22 | HR-ESI MS of 8. top. Experimental spectra of **8**. **top.** Theoretical spectra of **8**. **bottom.**

3.2.10 Characterisation of H_2N-F($C_{10}H_{21}$,Cy)-G($C_{10}H_{21}$,Cy)-F($C_{10}H_{21}$,Cy)NH 10:

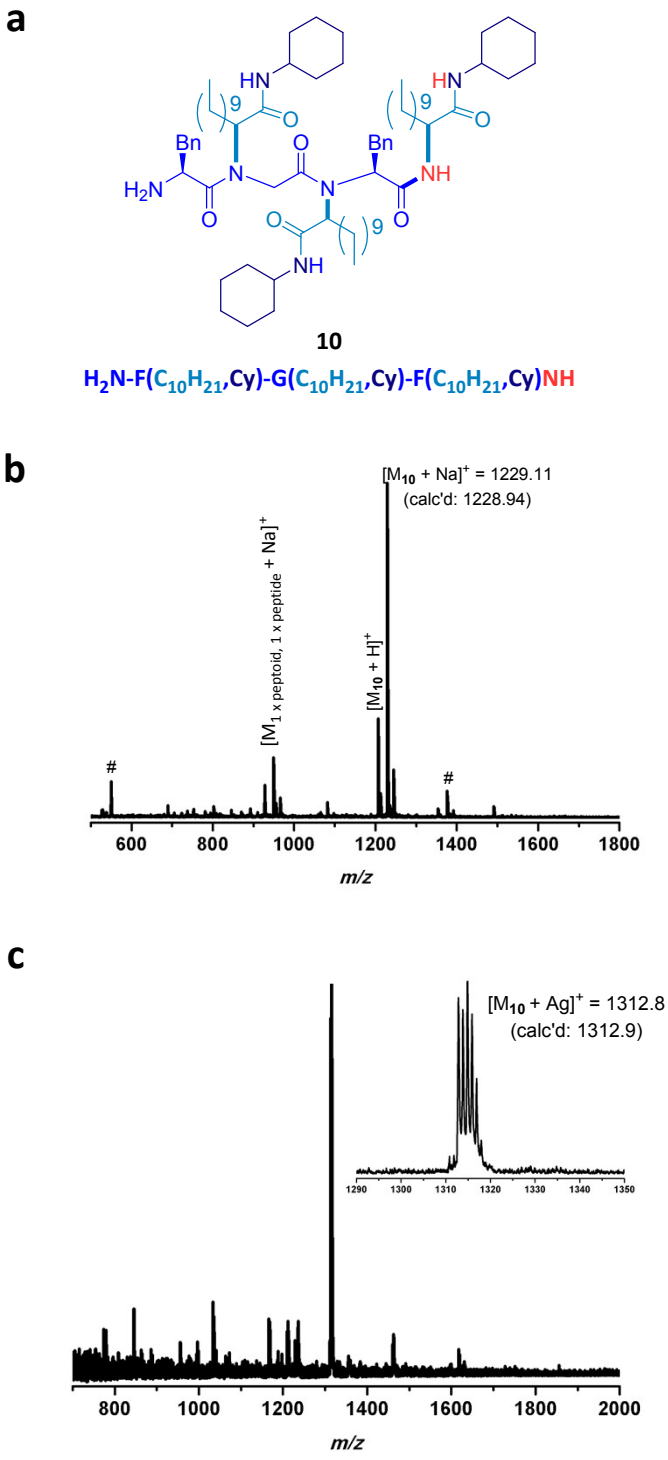

Figure S23 | Structure and characterisation of 10. a. Structure of compound **10**. **b.** Positive ESI-MS analysis of crude **10** after cleavage. **c.** MALDI-ToF analysis of crude **5** after cleavage using dithranol as matrix and Ag^+TFA^- as polarising agent.

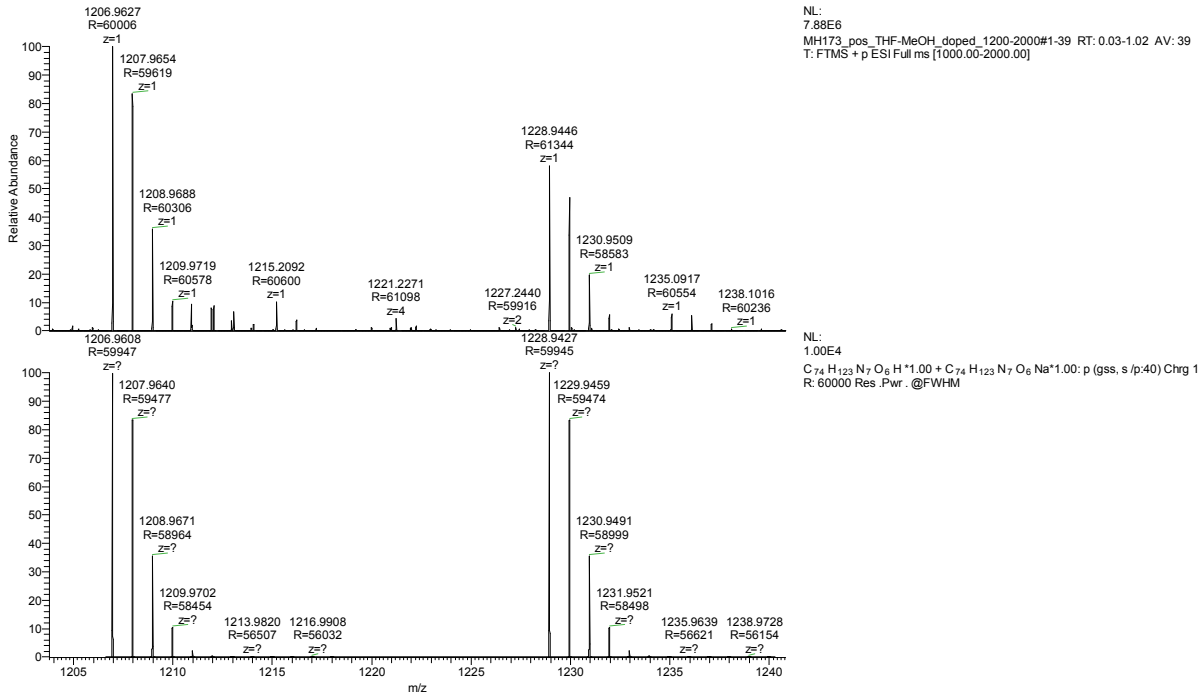

Peak	m/z exp	m/z theo	resolution	Δm
$[M + H]^+$	1206.9627	1206.9608	60 000	0.0019
$[M + Na]^+$	1228.9446	1228.9427	61 000	0.0019

Figure S24 | HR-ESI MS of 10. top. Experimental spectra of **10**. **top.** Theoretical spectra of **10**. **bottom.**

3.2.11 Characterisation of Fmoc-G($C_{10}H_{19}$,Cy)-G(*n*Pr,Cy)-F($C_{10}H_{21}$,Cy)-G($C_{10}H_{21}$,Cy)-F(*n*Pr,4-EM)- F($C_{10}H_{19}$,Cy)NH 11:

a

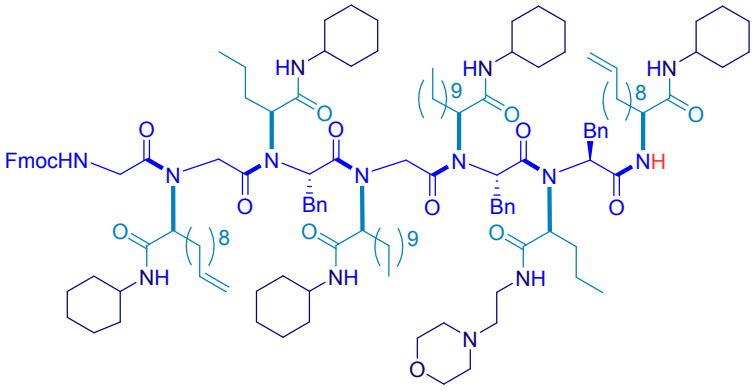

11

Fmoc-G($C_{10}H_{19}$,Cy)-G(*n*Pr,Cy)-F($C_{10}H_{21}$,Cy)-G($C_{10}H_{21}$,Cy)-F(*n*Pr,4-EM)- F($C_{10}H_{19}$,Cy)NH

b

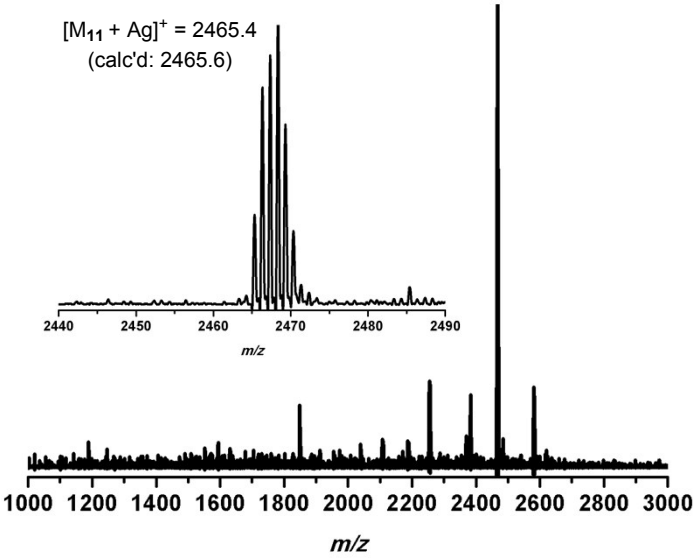

Figure S25 | Structure and characterisation of 11. a. Structure of compound **11**. **b.** MALDI-ToF analysis of crude **11** after cleavage using dithranol as matrix and Ag^+TFA^- as polarising agent.

3.2.12 Characterisation of H_2N-F($C_{10}H_{19}$,Cy)-(F($C_{10}H_{19}$,Cy))$_5$-F($C_{10}H_{19}$,Cy)NH 12:

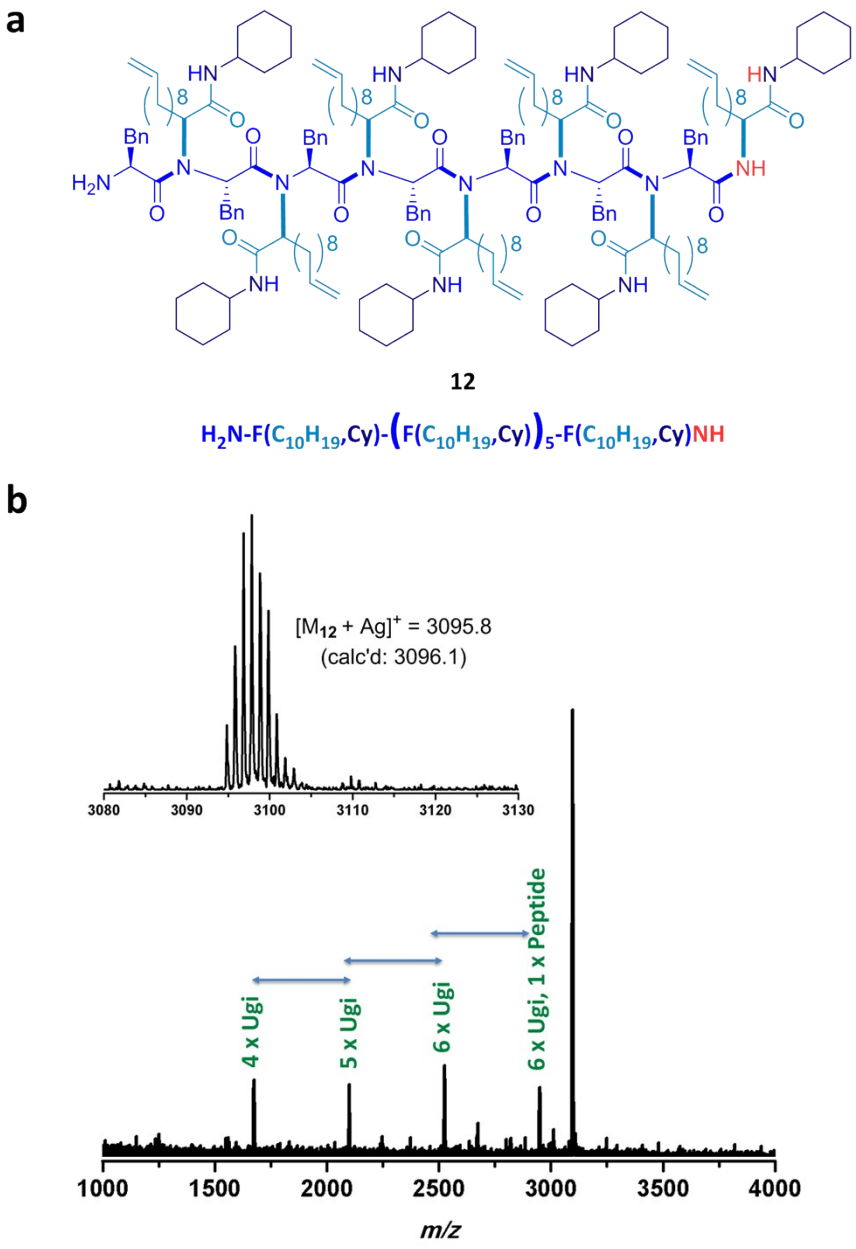

Figure S26 | Structure and characterisation of 12. a. Structure of compound **12**. **b.** MALDI-ToF analysis of crude **12** after cleavage using dithranol as matrix and Ag^+TFA^- as polarising agent.

4 Tandem MS analysis

4.1 Analysis of H_2N-F(*n*Pr,Cy)-F-G-F-$CONH_2$ 1:

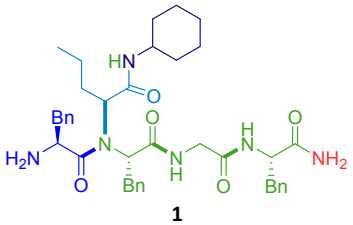

1

H_2N-F(*n*Pr_1,Cy)-F-G-F-$CONH_2$

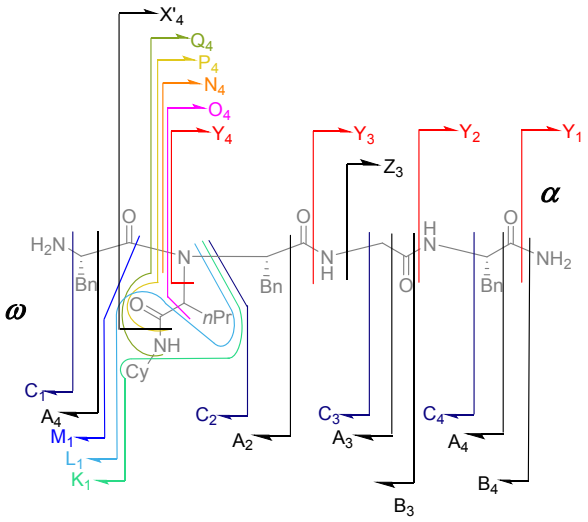

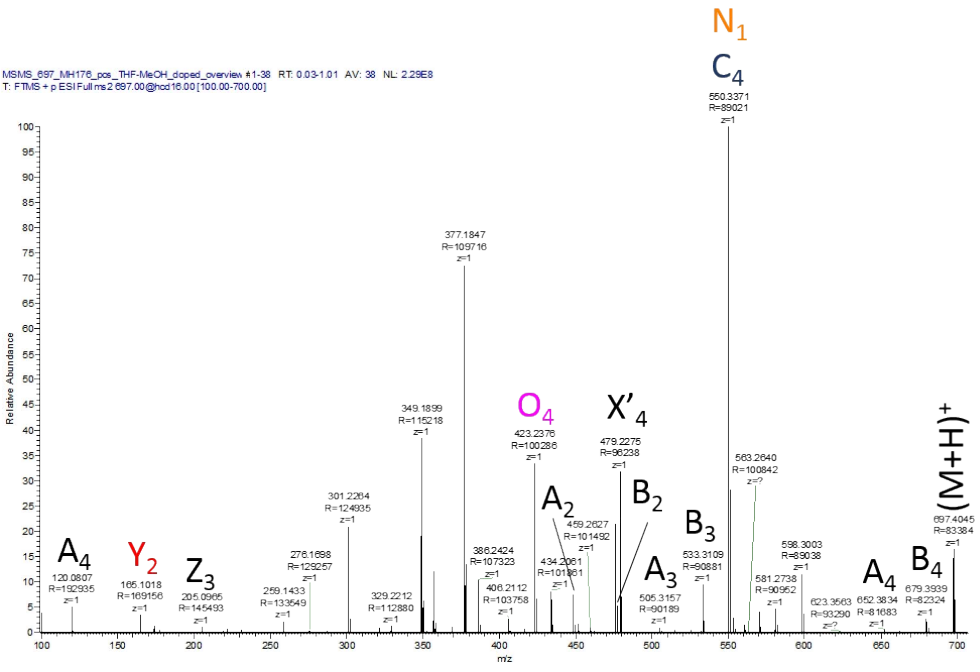

4.2 Analysis of H_2N-F($C_{10}H_{21}$,Cy)-F-G-F-$CONH_2$ 2:

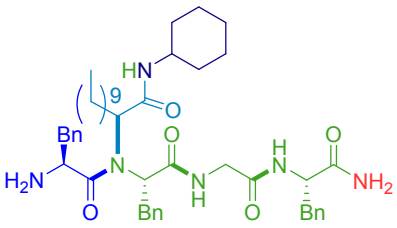

2

H_2N-F($C_{10}H_{21}$,Cy)-F-G-F-$CONH_2$

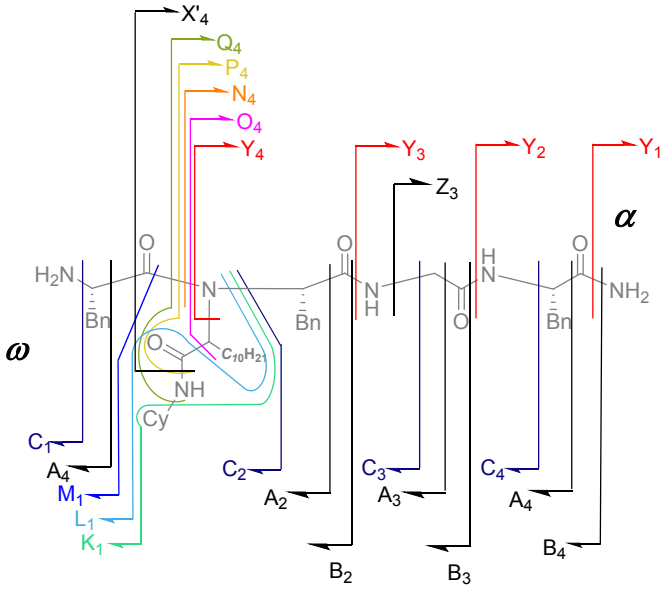

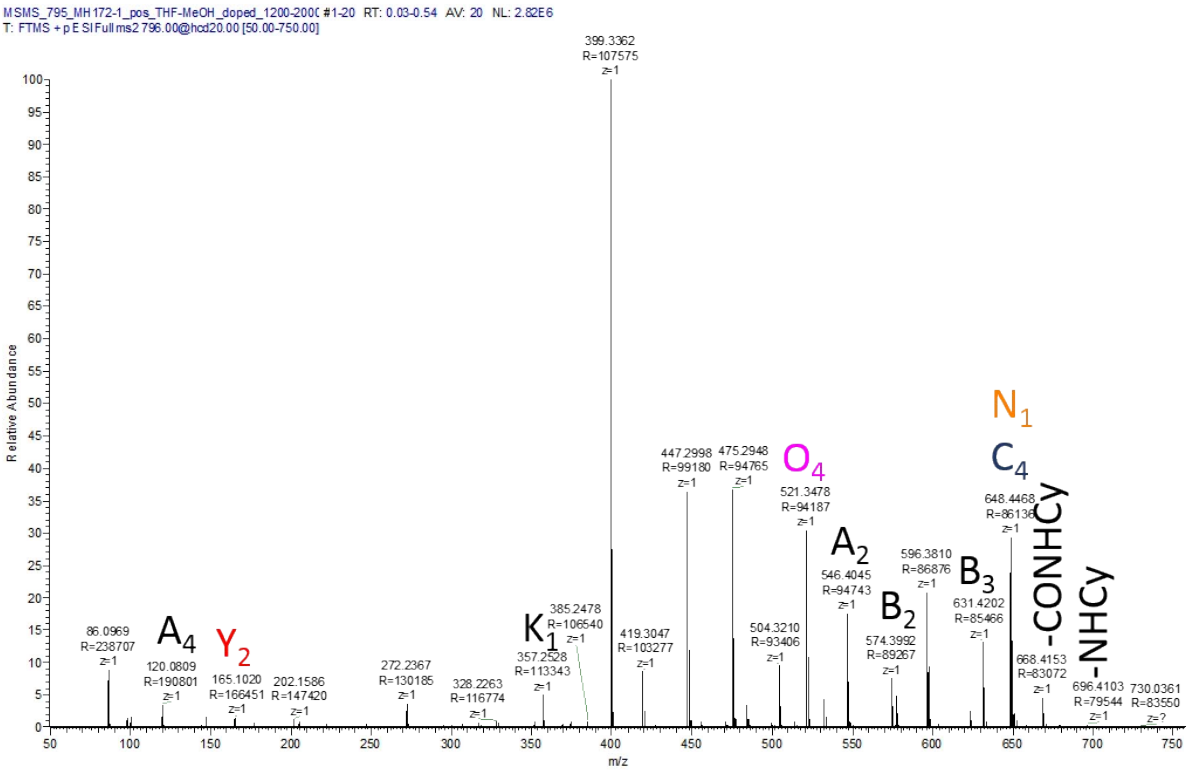

4.3 Analysis of H_2N-F-F(*n*Pr,Cy)-K-K-K-K-$CONH_2$ 3:

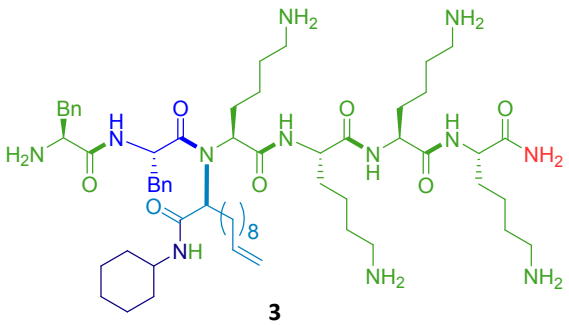

3

H_2N-F-F(*n*Pr,Cy)-K-K-K-K-$CONH_2$

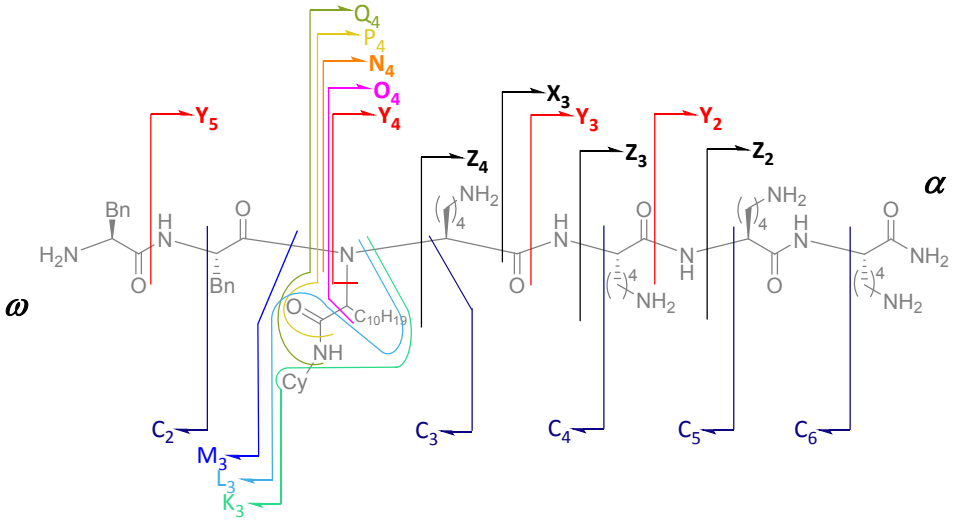

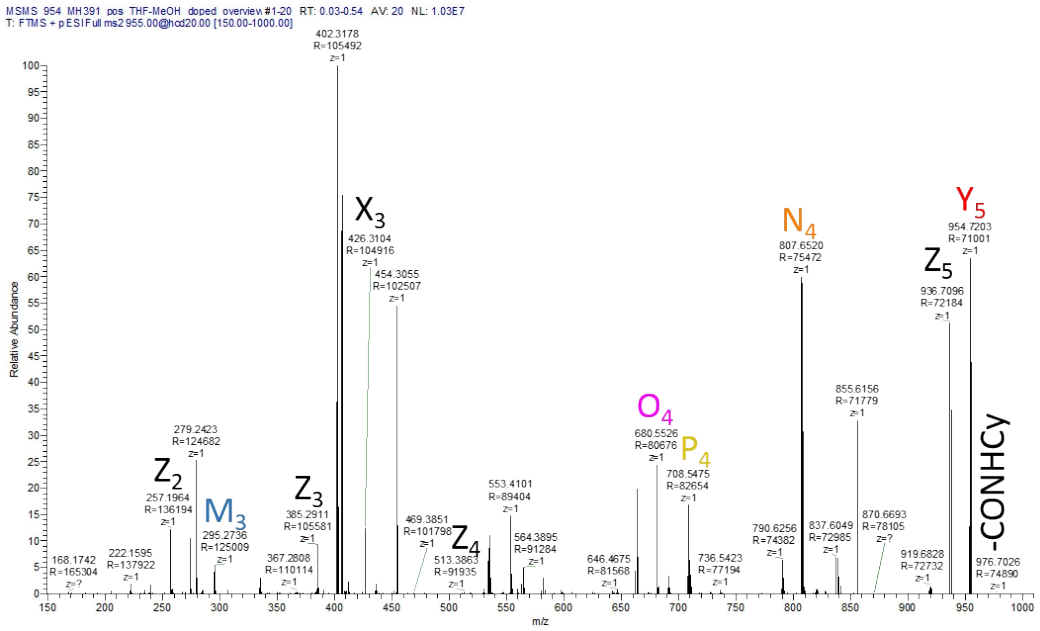

4.4 Analysis of H_2N-F($C_{10}H_{21}$,Cy)-F-F(*n*Pr,Cy)-F-F($C_{10}H_{21}$,Cy)-F-G-F-$CONH_2$ 7:

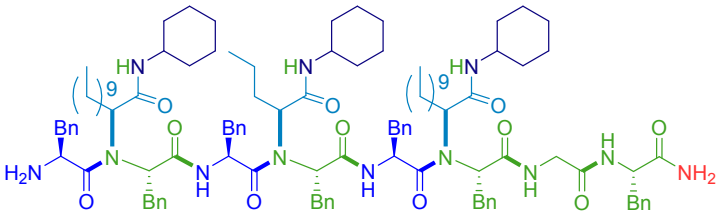

7

H_2N-F($C_{10}H_{21}$,Cy)-F-F(*n*Pr,Cy)-F-F($C_{10}H_{21}$,Cy)-F-G-F-$CONH_2$

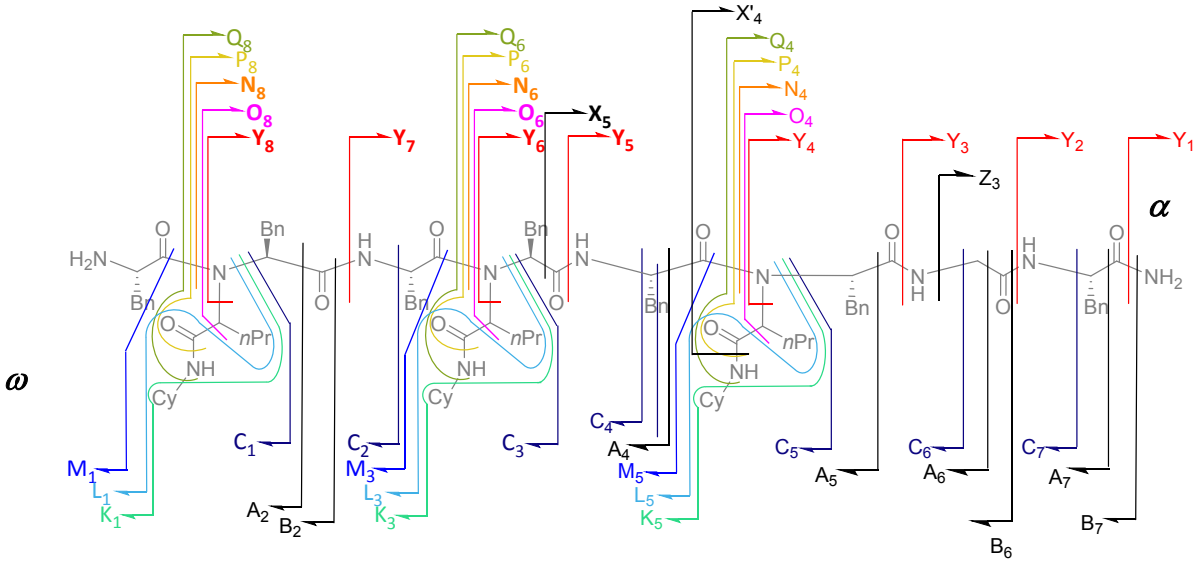

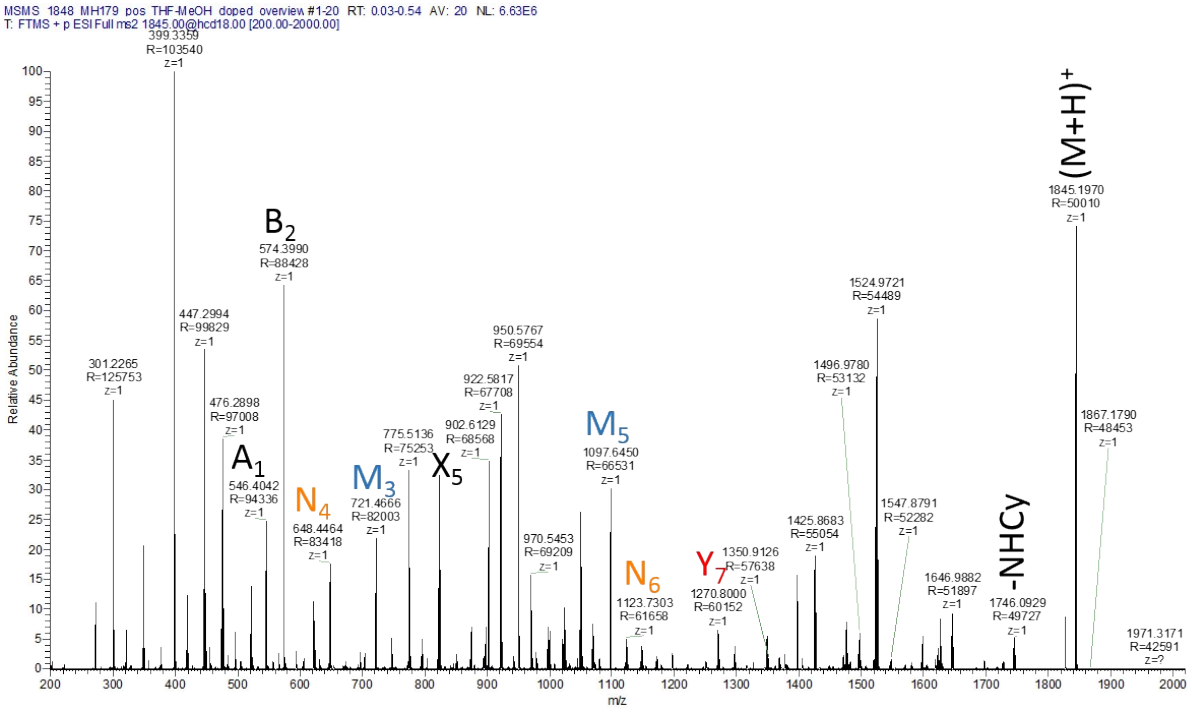

4.5 Analysis of Fmoc-F(*n*Pr,Cy)-F-F(*n*Pr,Cy)-F-F(*n*Pr,Cy)-K-K-K-K-$CONH_2$ 8:

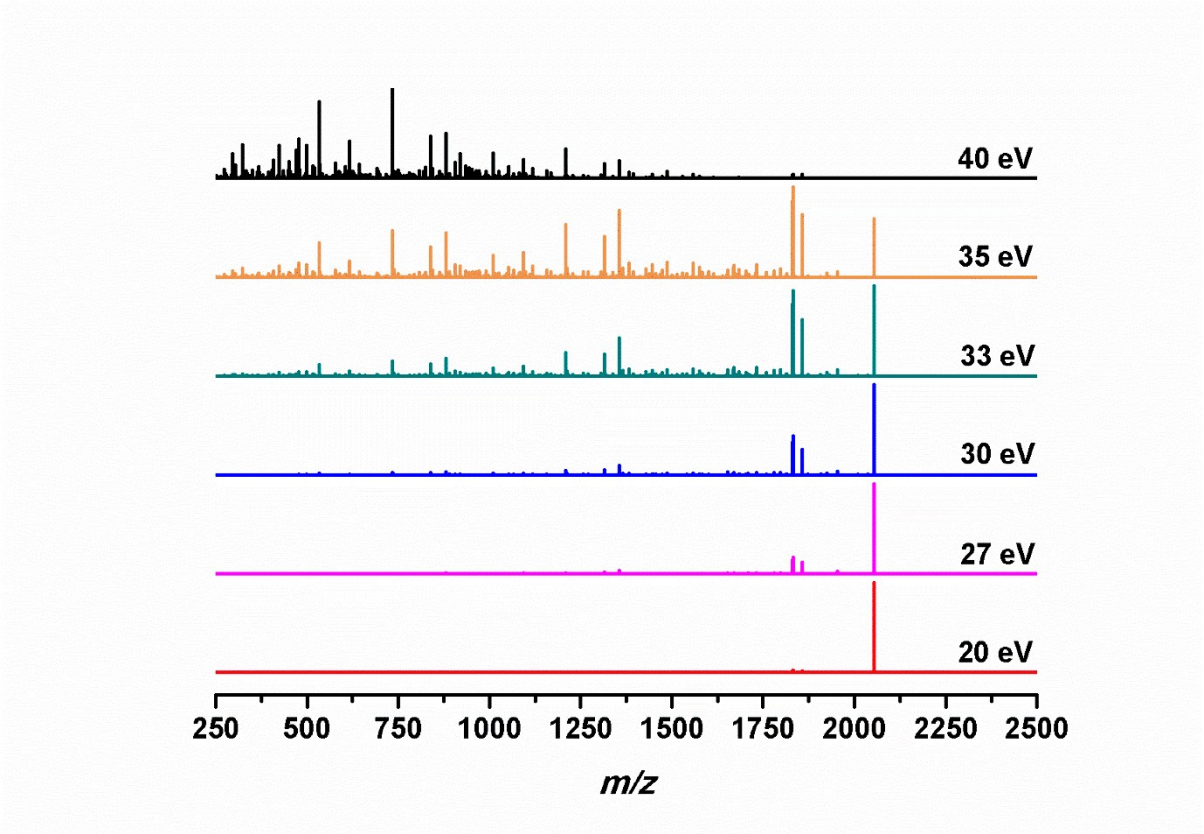

Figure S27 | MS/MS analysis of 8 at different eV.

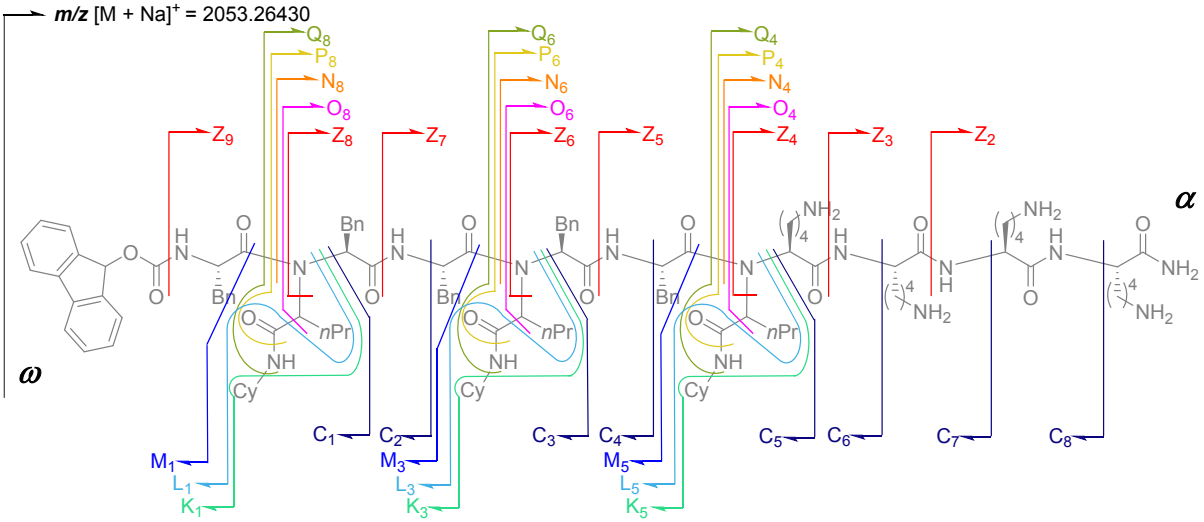

Figure S28 | Schematic presentation of oligomer 8 and its assignment into different fragmentation patterns.

Table S1 | Experimental and theoretical *m/z* of MS/MS fragments of compound 8.

Fragment	*m/z* [g·mol]		Fragment	*m/z* [g·mol]	
	Exp.	Theo.		Exp.	Theo.
C_1	590.30	590.30	**N_4**	733.54	733.54
C_2	737.37	737.37	**N_6**	1208.82	1208.83
C_3	1065.66	1065.68	**N_8**	1685.09	1685.11
C_4	1212.65	1212.65	**O_4**	607.40	607.45
C_5	1541.97	1541.87	**O_6**	1082.73	1082.72
C_6	1668.97	1668.96	**O_8**	1557.97	1558.02
C_7	1797.07	1797.05	**P_4**	634.44	634.44
C_8	1925.16	1925.15	**P_6**	1109.72	1109.72
K_1	507.29	507.21	**P_8**	1585.01	1585.00
K_3	982.52	982.50	**Q_4**	650.40	650.46
K_5	1457.90	1457.78	**Q_6**	1125.69	1125.74
L_1	463.20	463.20	**Q_8**	1600.97	1601.02
L_3	938.48	938.48	**Z_2**	296.20	296.21
L_5	1413.77	1413.77	**Z_3**	423.21	423.29
M_1	394.20	394.20	**Z_4**	551.33	551.38
M_3	869.49	869.42	**Z_5**	880.61	880.61
M_5	1344.75	1344.71	**Z_6**	1025.67	1025.66
			Z_7	1355.89	1355.90
			Z_8	1500.95	1500.95
			Z_9	1831.20	1831.18

4.6 Analysis of H_2N-K(CH_2)$_2$-S-Glu),Cy)-K(CH_2)$_2$-S-Glu),Cy)-K(CH_2)$_2$-S-Glu),Cy)-K-K-K-K-$CONH_2$ 9:

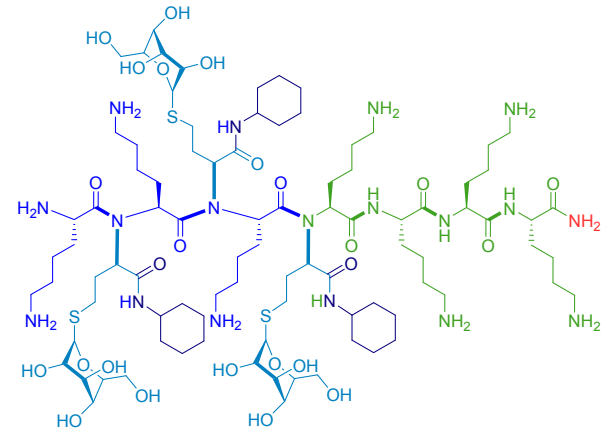

9

H_2N-K(CH_2)$_2$-S-Glu),Cy)-K(CH_2)$_2$-S-Glu),Cy)-K(CH_2)$_2$-S-Glu),Cy)-K-K-K-K-$CONH_2$

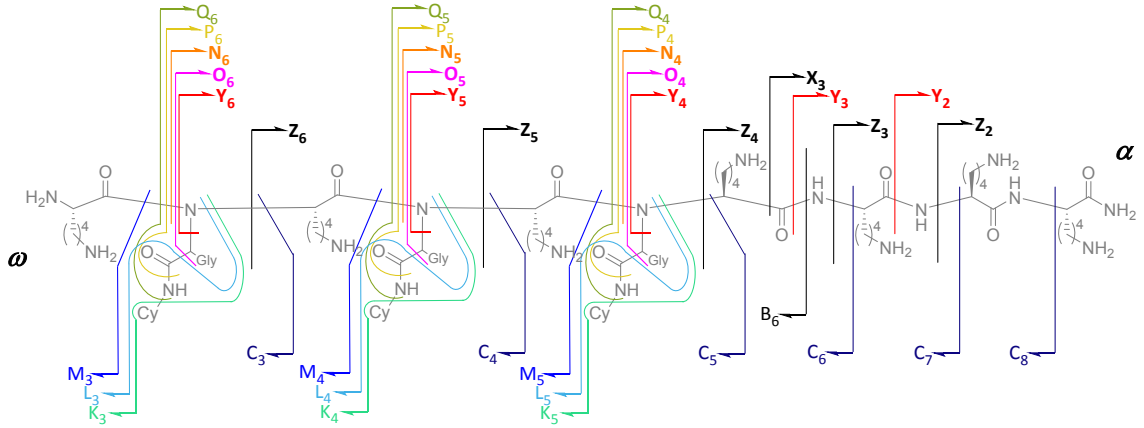

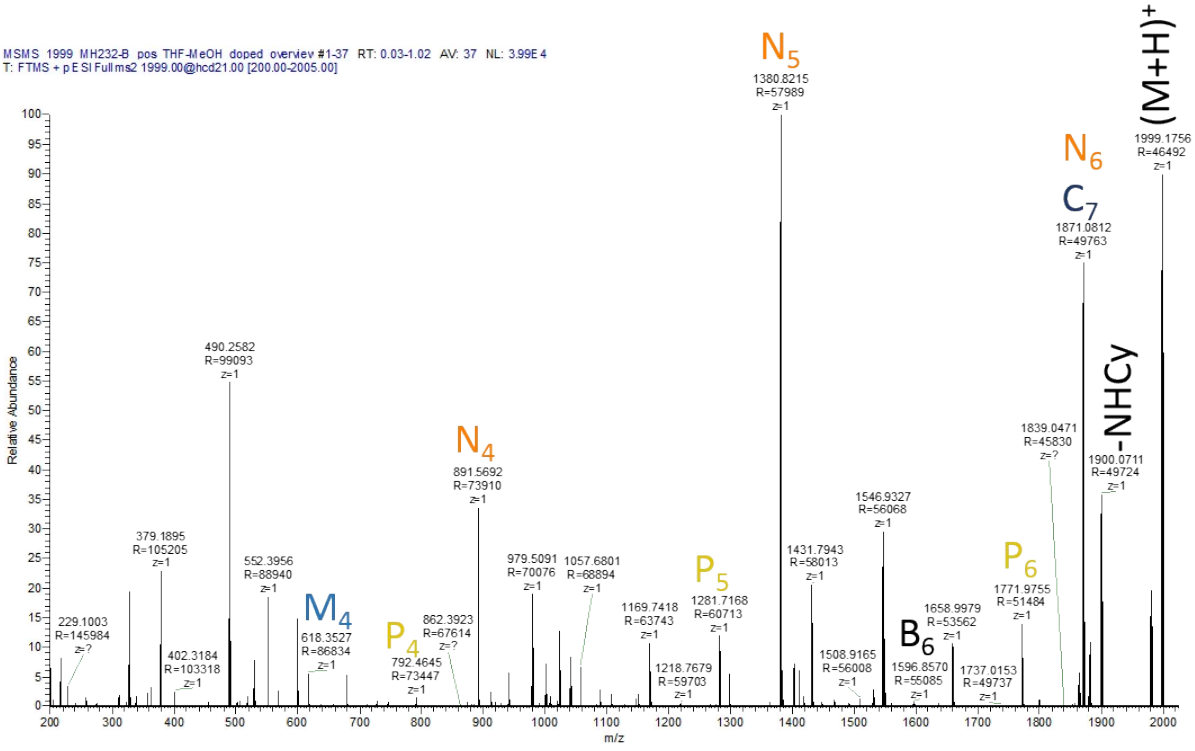

4.7 Analysis of H_2N-F($C_{10}H_{21}$,Cy)-G($C_{10}H_{21}$,Cy)-F($C_{10}H_{21}$,Cy)NH 10:

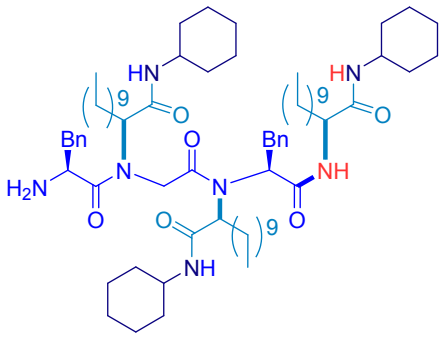

10

H_2N-F($C_{10}H_{21}$,Cy)-G($C_{10}H_{21}$,Cy)-F($C_{10}H_{21}$,Cy)NH

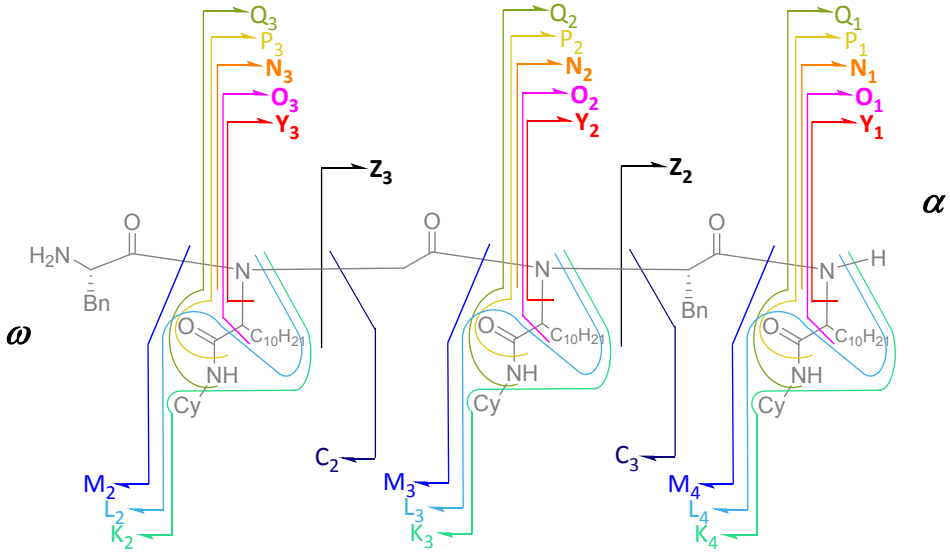

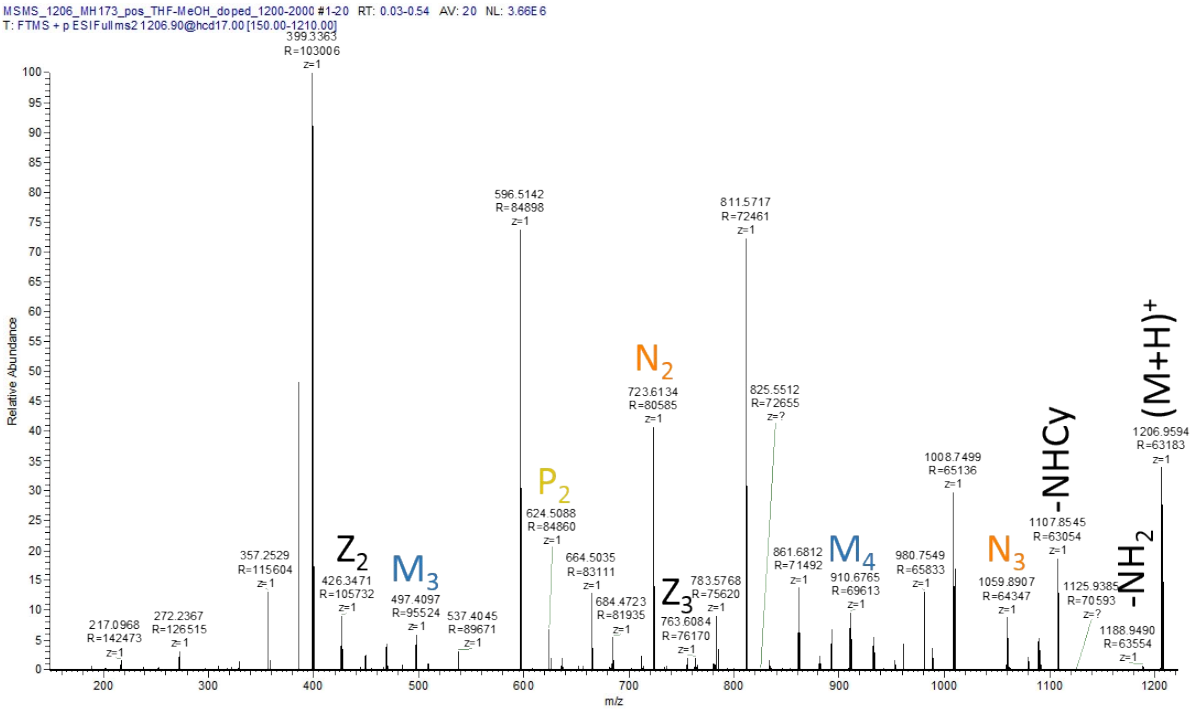

5 Assembly studies

Table S2| SAXS form factor fit parameters of compound 3 and 5[a]

Sample	Mass Fraction Gaussian			Generalised Gaussian coil				BG
	R_g	D	I_0	R_g	N_u	I_0	N	
Compound 3	234.8	3.5	0.57	6.83	0.388	0.0024	0.76	7.2×10^{-4}
Compound 5	165.0	1.98	0.02	7.62	0.205	0.0027	1.47	2.07×10^{-3}

[a] Fitted to monodisperse fractal form factor and a Gaussian generalised coil using SASfit. R_g = Radius of gyration. D = fractal dimension. I_0 = forward scattering. N_u = Flory Exponent. N = scaling factor. BG = background.

Table S3 | SAXS form factor parameters of compound 8[b]

Sample	η_{shell}	BG	R_1	R_2	mu	Gaussian		
						N	S	X_0
Compound 8	3.04×10^{-6}	1.14×10^{-3}	10	7.93	-1.3	0.61	6.57	33.07

[b] Fitting to 'spherical shell' model using SASFIT. η_{shell} = scattering contrast of the shell. BG = Background. R_1 = Outer radius (fixed) R_2 = inner radius of the shell. mu = parameter effecting the scattering of the inner core (mu* η_{shell} = η_{core}. N = Scaling factor. X_0 and S = Gaussian polydispersity parameters.

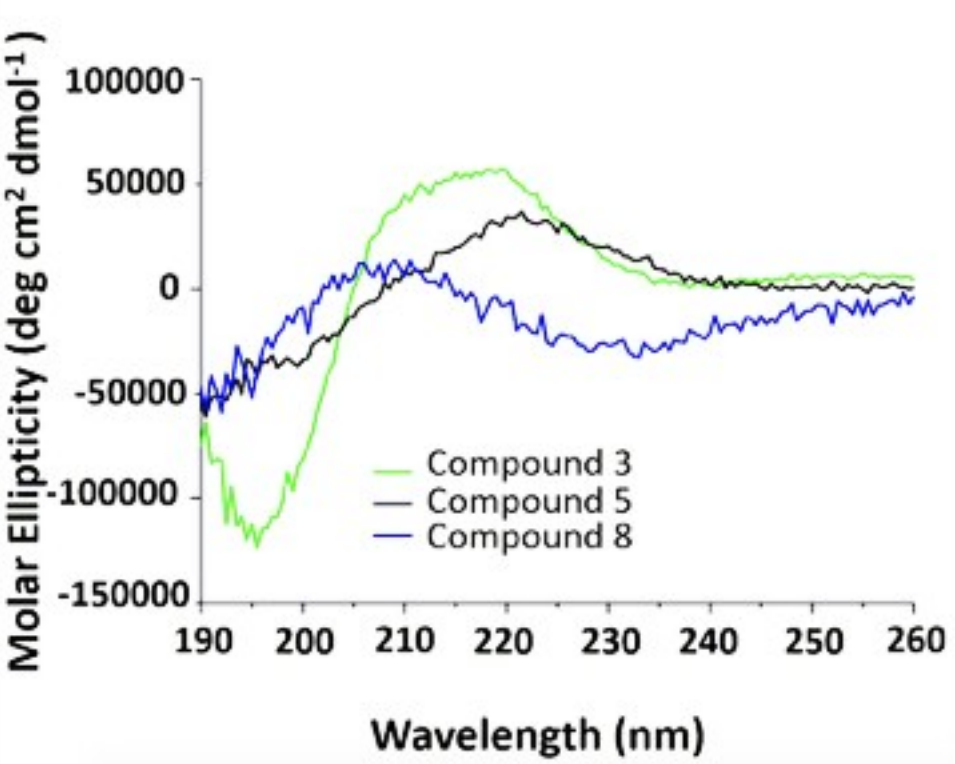

Figure S29. CD Spectrum of compound 3, 5, and 8.

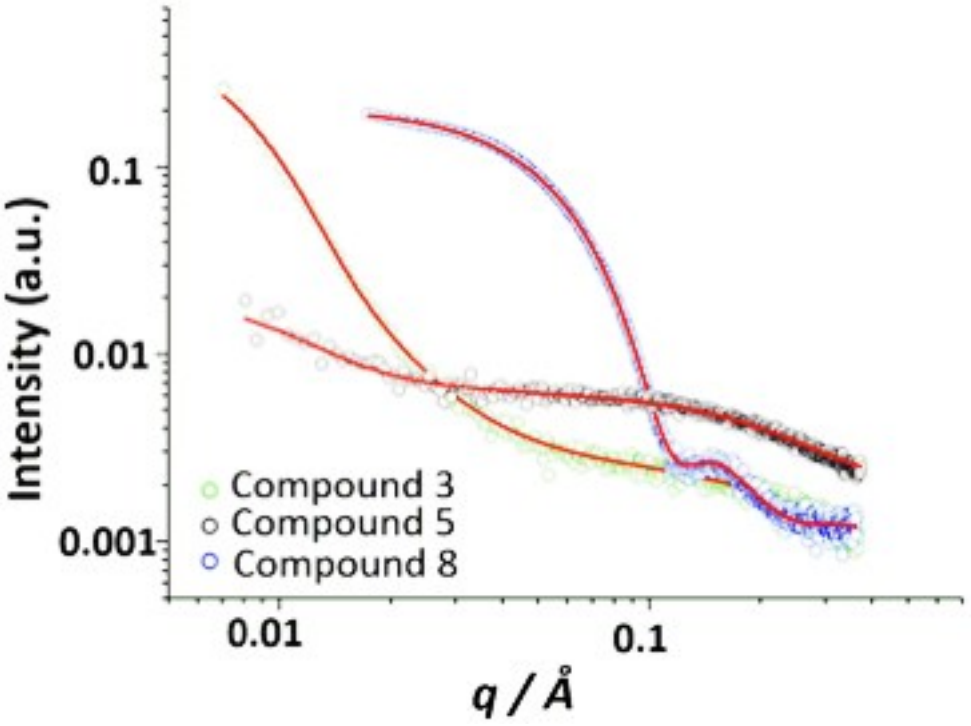

Figure S30. SAXS data of compound 3, 5, and 8.